

Revised timing and onset location of two isolated substorms observed by Time History of Events and Macroscale Interactions During Substorms (THEMIS)

J. Liu,¹ V. Angelopoulos,¹ M. Kubyshkina,² J. McFadden,³ K.-H. Glassmeier,^{4,5} and C. T. Russell¹

Received 30 June 2010; revised 27 September 2010; accepted 2 November 2010; published 8 January 2011.

[1] We report timing analysis on two previously published substorm events captured by the Time History of Events and Macroscale Interactions During Substorms (THEMIS) spacecraft. During the 29 January 2008 0713 UT substorm, the solar wind velocity had a strong southward component corresponding to a 6.5° southward tilt of the magnetotail. Viewed in a rotated system, the magnetic field at the most distant probe, P1 ($X_{GSM} = -29.5 R_E$), shows a bipolar magnetic signature interpreted herein as a tailward moving plasmoid; P2 ($X_{GSM} = -18.5 R_E$) also observed magnetic signatures indicating tailward motion at onset. P3 ($X_{GSM} = -10.8 R_E$) and P4 ($X_{GSM} = -10.6 R_E$) captured dipolarization fronts and earthward flows at the same time. After allowing for the more general case of different magnetosonic speeds on the two sides of the reconnection site, timing of the first signatures in space and ground reveals that tail reconnection initiated at $\sim 18 R_E$ down tail, ~ 2 min prior to auroral intensification. Allowing for different magnetosonic speeds on either side of the reconnection site is warranted by the large separation between the inner ($10\text{--}12 R_E$) and outer ($25\text{--}30 R_E$) probe locations and differing ion temperatures and equatorial magnetic fields expected at those locations. The same technique was applied for the 2 February 2008 0740 UT substorm event during which midtail data from P2 were unavailable. A previous study obtained a reconnection site location of $X_{GSM} = -11\text{--}17 R_E$ assuming the same propagation speed on both sides of the reconnection site. Relaxation of the constant-speed condition results in a reconnection location of $\sim 22 R_E$ and an inferred reconnection time of $\sim 3\text{--}4$ min before the auroral intensification. Our results are consistent with other THEMIS event studies that are unaffected by large solar wind deflections or incomplete probe coverage, suggesting that reconnection triggering of substorm onset is a common occurrence.

Citation: Liu, J., V. Angelopoulos, M. Kubyshkina, J. McFadden, K.-H. Glassmeier, and C. T. Russell (2011), Revised timing and onset location of two isolated substorms observed by Time History of Events and Macroscale Interactions During Substorms (THEMIS), *J. Geophys. Res.*, 116, A00I17, doi:10.1029/2010JA015877.

1. Introduction

[2] Substorms are global reconfigurations of the magnetosphere involving solar wind energy storage in Earth's magnetotail and abrupt conversion of this energy into particle heating and kinetic energy [Akasofu, 1964; Axford, 1999].

Substorms are responsible for various well-documented magnetotail and ground phenomena. Satellites in the magnetotail at $6\text{--}10 R_E$ observe strong dipolarization interpreted as a substorm current wedge [McPherron, 1979]. A reduction in cross-tail current during substorms is observed as an increase in the Z component of the magnetic field, often accompanied by a decrease in the X component [Lopez and Lui, 1990], signifying that the field is changing from tail-like to dipole-like (a dipolarization). Occasionally a large increase in B_z is preceded by a small decrease in B_z , which has been attributed to explosive buildup of the cross-tail current prior to its relaxation near substorm onset [Ohtani et al., 1992]. Further down tail at $8\text{--}20 R_E$, transient dipolarizations and earthward flows (known as bursty bulk flows) are seen frequently during active times, including substorms [Angelopoulos et al., 1994]. Occasionally magnetic field bipolar signatures in the Z_{GSM} direction, associated with earthward flows, are seen

¹IGPP/ESS, University of California, Los Angeles, California, USA.

²Institute of Physics, St. Petersburg State University, St. Petersburg, Russia.

³Space Sciences Laboratory, University of California, Berkeley, California, USA.

⁴Institute for Geophysics and Extraterrestrial Physics, Technische Universität Braunschweig, Braunschweig, Germany.

⁵Max Planck Institute for Solar System Science, Katlenburg-Lindau, Germany.

near the substorm onset region; these are sometimes interpreted as earthward moving flux ropes [Ohtani *et al.*, 1992; Eastwood *et al.*, 2005].

[3] Further down tail, tailward moving plasmoids associated with substorms [Hones, 1980; Slavin *et al.*, 1984], also known as nightside flux transfer events (NFTEs) [Sergeev *et al.*, 1992], have been observed near the neutral sheet in association with substorms. When observed near the plasma sheet boundary layer or the lobes, these have been termed traveling compression regions or TCRs [Slavin *et al.*, 1984]. The sense of the bipolar signature depends on the location of the satellites relative to the reconnection site: positive-then-negative B_z is observed for a tailward moving NFTE, whereas negative-then-positive B_z is observed for an earthward moving NFTE. It is expected that a fully formed NFTE can be observed even far enough from the reconnection site. Flows accompanying the reconnection process are away from the reconnection site when observed near the neutral sheet [Hayakawa *et al.*, 1982; Nishida *et al.*, 1981; Hones, 1980; Nagai, 2006] and toward the neutral sheet when observed at the plasma sheet boundary layer [Angelopoulos *et al.*, 2009]. Closer to the reconnection site, a deflection of the tail field consistent with magnetic reconnection is expected, i.e., a northward deflection of the field earthward of the reconnection site, and a southward deflection on the tailward side of the reconnection site. Near the neutral sheet, these magnetic deflections ought to be accompanied by flows away from the reconnection site, whereas near the lobes they are expected to be associated with flow toward the reconnection site, as predicted by typical reconnection topology.

[4] One of the most defining aspects of a substorm is the auroral intensification and poleward expansion [Akasofu, 1964]. The ground signatures of auroral substorms consist of rapid auroral intensification, breakup of auroral forms into smaller filaments, poleward expansion, and a westward surge of the most intense auroral arcs. Auroral activity is associated with ionospheric currents that cause ground magnetic signatures, including an abrupt increase in the auroral electrojet (AE) index and irregular magnetic field pulsations in the 40–150 s range, called Pi2 pulsations [Jacobs *et al.*, 1964; Saito, 1969].

[5] Until very recently, the mechanism that triggers substorms was still in dispute. There are two main models for substorms: the current sheet disruption model [Lui, 1996] and the near-Earth neutral line model [Baker *et al.*, 1996]. The current sheet disruption model asserts that when the current sheet thins, the ions become nonadiabatic and begin to stream across the current sheet in serpentine orbits and interact with adiabatic electrons drifting in the opposite direction, producing low-frequency whistler-type waves at $\sim 10 R_E$. These waves cause the plasma sheet to act resistively, disrupting the cross-tail current. This process produces a rarefaction wave that propagates down the tail, which, in turn causes the reconnection signatures typically observed at 20–30 R_E . The near-Earth neutral line model postulates that reconnection occurring at the current sheet at 20–30 R_E [Nagai *et al.*, 1998; Nagai *et al.*, 2005; Ge and Russell, 2006] is destabilized by either an external (solar wind) or internal (magnetotail) process. Reconnection produces earthward flows and tailward moving plasmoids. The earthward flows interact

with the near-Earth region, producing intense field-aligned currents [Shiokawa *et al.*, 1997; Birn *et al.*, 1999; Zhang *et al.*, 2007] that cause auroral intensification. Dipolarization at 10 R_E and reconnection at 20–30 R_E are connected by waves, and the communication time between these regions is on the order of 60 s. The communication time to the ionosphere from either location is between 60 and 120 s.

[6] The Time History of Events and Macroscale Interactions During Substorms (THEMIS) mission [Angelopoulos, 2008; Angelopoulos *et al.*, 2008a; Sibeck and Angelopoulos, 2008] was designed to discover which substorm onset mechanism is supported by the data and the causal connection between different parts of the magnetosphere. It employs five satellites (probes) in orbits that enable them to align parallel to the Sun–Earth line once every 4 days. Thus, they can monitor tail phenomena simultaneously between $\sim 10 R_E$ and ~ 20 –30 R_E down tail. A network of ground-based observatories (GBOs) is also deployed to determine the meridian and onset time of Pi2 pulsations and auroral intensifications [Mann *et al.*, 2008; Mende *et al.*, 2008; Russell *et al.*, 2008]. Recent THEMIS observations [Angelopoulos *et al.*, 2008b; Gabrielse *et al.*, 2009; Liu *et al.*, 2009; Pu *et al.*, 2010] indicate that substorm onset is triggered by reconnection which begins at $\sim 20 R_E$ down tail, approximately 2–3 min prior to ground auroral intensification onset. Earlier observations of ground auroral signatures of magnetotail flows [Zesta *et al.*, 2000; Sergeev *et al.*, 2000; Zesta *et al.*, 2006] demonstrated that north–south arcs are associated with such flows and that occasionally such flows protrude very close to the inner magnetosphere. In many instances north–south arcs are associated with poleward boundary intensifications. More recent observations using the ground-based THEMIS array of north–south arcs [Lyons *et al.*, 2010; Nishimura *et al.*, 2010] showed that north–south arcs protruding to the equatorward edge of the auroral oval correlate well with an ensuing substorm auroral intensification. Thus, there is mounting evidence both in the ionosphere and in space of reconnection processes triggering energization of the inner magnetosphere that results in the global substorm onset instability.

[7] However, two studies during the early THEMIS period presented a different scenario for substorm onset, one that favors a near-Earth initiation, i.e., a current disruption process preceding reconnection. These events occurred on 29 January 2008 and 2 February 2008, and were studied by Lui *et al.* [2008] and Mende *et al.* [2009], respectively. Like many substorms, these also consist of multiple successive activations of the auroral oval. Because plasma sheet disturbances from the initial activation precondition both the tail with localized dipolarized flux and flows, and the ionosphere with enhanced conductance and gradients, it is important to establish accurately the timing history of the first substorm activation in each series.

[8] Investigating the two initial events of each activation sequence with further scrutiny, we find that tail reconnection is a likely hypothesis for both events, but because of the midtail satellite positions at large distance to the neutral sheet and also because of the special circumstances surrounding each event, this realization was not possible until now.

[9] In sections 2–5 we will first introduce our new timing results for the two substorm events and then determine the

reconnection site and time of the two events allowing for a (more general) hypothesis of different propagation speeds on the two sides of the reconnection site.

2. Instrumentation

[10] THEMIS, launched on 17 February 2007, consists of five identical satellites (probes) equipped with comprehensive particle and field instruments used to determine the onset mechanism of substorms by aligning probes along the magnetotail plasma sheet and timing the propagation time delays between different points in the magnetosphere and the ionosphere [Angelopoulos, 2008]. The five probes traveled through the magnetotail with different apogees [Sibeck and Angelopoulos, 2008]: Probe 1 (P1) had an apogee of $\sim 30 R_E$; P2, $\sim 20 R_E$; P3 and 4; $\sim 12 R_E$, and P5, $\sim 10 R_E$. (Note that the probe names are also given in letters: B, C, D, E, A corresponding to 1, 2, 3, 4, 5; that is, the letter sequence matches the number sequence after cyclical permutation by one letter position). The probe apogees and active control of in-orbit phasing enable probe observations of the same event in alignment at various altitudes; such alignments are timed to be between 0000 and 1200 UT, when the North American continent is over the nightside. Twenty THEMIS ground-based observatories (GBOs) [Mende et al., 2008], deployed from eastern Canada to western Alaska (several of these stations are part of the CARISMA (<http://www.carisma.ca>) [Mann et al., 2008] and GIMA (<http://magnet.gi.alaska.edu/>) magnetometer arrays), provide all-sky aurora imagers and ground magnetic field data. An additional 11 education and public outreach (EPO) magnetometers [Russell et al., 2008] deployed across the United States complement the ground magnetometer array with subauroral and midlatitude observations. A map of these stations is shown in Figure S1 in Text S1.¹ These observatories help determine the onset of auroral intensification, negative bays and ULF waves.

[11] Observations from December 2007 to April 2008, constitute the first tail season for THEMIS alignments. During that period the nominal distance from the neutral sheet for the outer probes (P1, P2) was held at $<5 R_E$ to determine the onset of particle acceleration in the midtail from plasma sheet boundary layer beams or currents. In retrospect, the outer probe signatures of plasma sheet boundary beams and flows were scarce near onset, whereas bipolar fields (TCRs/NFTEs) dominated the midtail signatures of onset. This was attributed to extreme plasma sheet thinning during substorm onset. For the second season (December 2008 to May 2009), the orbit was changed with a stricter criterion of P1, P2 proximity to within $<2 R_E$. This yielded a similar number of substorm observations from close proximity to the neutral sheet, because of the reduced solar activity (prolonged solar minimum) during the second tail season. The two substorms studied herein are from the first half of the first tail season when P1, P2 were at relatively far from the neutral sheet ($\sim 5 R_E$) slightly to the postmidnight sector in aberrated magnetospheric coordinates.

[12] In this paper we revisit the analysis of the two events using data from the Fluxgate Magnetometer (FGM) instrument [Auster et al., 2008] and Electro-Static Analyzer (ESA) instrument [McFadden et al., 2008]; the latter measures 0–

25 keV particles on the THEMIS probes. We also used All-Sky Imager (ASI) [Mende et al., 2008] and Ground Fluxgate Magnetometer (GMAG) data [Russell et al., 2008; Mann et al., 2008]. Finally, we used ground magnetometer data from the midlatitude Intermagnet network for contextual observations of ring current, partial ring current, and substorm current wedge intensities.

3. The 29 January 2008 Event

[13] The 29 January event consists of three successive substorms: at ~ 0714 UT, at ~ 0742 UT and at ~ 0828 UT. The reader is referred to the Lui et al. [2008] paper for spacecraft positions, particle spectra, and individual ASI imager plots, as well as a detailed description of the second and third intensifications. Overview plots and mosaic images and movies are available on the THEMIS website (<http://themis.ssl.berkeley.edu/>; see Data tab, then Summary Plots) provide contextual information. Here we only look at the first substorm at ~ 0714 UT and focus on timing-related signatures of that onset that were either not available in the Lui et al. [2008] work or are required to make this paper self-sufficient.

3.1. Ground Signatures

[14] On 29 January 2008 at around 0714 UT, the all-sky imagers at Inuvik (magnetic latitude 68.413N, longitude 226.230E), Fort Simpson (magnetic latitude 61.762N, longitude 238.779E) and Fort Smith (magnetic latitude 59.984N, longitude 248.158E) captured the auroral intensification and expansion related to this event. A sequence of high-resolution all-sky images of Inuvik, Fort Simpson, and Fort Smith from 0711 UT to 0718 UT is shown in Figure 1. The auroral intensification was seen first at Fort Smith (Figure 1b). A noticeable preexisting arc within the field of view of Inuvik at magnetic latitude ~ 68 N faded soon after the auroral intensification. The integrated auroral intensity over the red rectangle portion (Figure 1b) of the field of view at Fort Smith is shown in Figure 2a, on a log scale (arbitrary units). The integrated auroral intensity increased very gradually initially, but after $\sim 0712:22$ UT the increase was quite rapid. The dashed vertical line in Figure 2a is determined to be the inflection point on this logarithmic intensity time series plot. Thus, we take this instance to be the time of auroral intensification, consistent with Angelopoulos et al. [2008b]. Our auroral intensification time is different from the time (0714 UT) selected by Lui et al. [2008], who determine the time directly from all-sky images. This is due to our approach of using the integrated auroral intensity over the region of interest (consistent with Angelopoulos et al. [2008b], Gabrielse et al. [2009], and Liu et al. [2009]), resulting in higher sensitivity and allowing us to clearly differentiate between the exponential intensity increase and the linear growth in the substorm growth phase. The arc began to expand westward and reached the field of view of Fort Simpson (Figure 1c) and Inuvik (Figure 1d) successively. The arc also expanded poleward after 0713:51 UT inside the field of view of Fort Smith. It continued to brighten and expand westward and poleward after 0717:42 UT (Figure 1f), and reached $\sim 2^\circ$ north of the original latitude of the intensification. This poleward expansion qualifies the event to be a substorm (though a small one) [Rostoker et al., 1980] rather

¹Auxiliary materials are available in the HTML. doi:10.1029/2010JA015877.

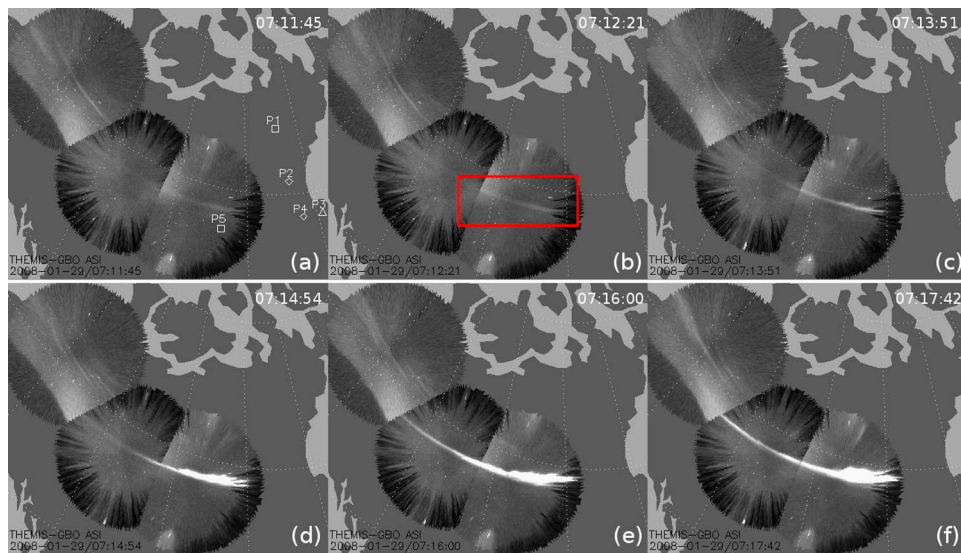


Figure 1. All-sky imagers' aurora photographs of the 29 January event at (from west to east) Inuvik, Fort Simpson, and Fort Smith. The red square is the integration area in Figure 2a.

than a pseudo breakup. It is noted, however, that even though what constitutes a substorm versus a pseudo breakup is a matter of a rather arbitrary definition on the extent of the poleward expansion, even pseudo breakups have been shown to have similar magnetospheric signatures as substorms and one can hardly tell them apart from spacecraft observations [Angelopoulos *et al.*, 1995; Aikio *et al.*, 1999].

[15] Figures 2b–2e show observations of geomagnetic activity by the THEMIS GBOs as a function of time. High-latitude stations Fort Simpson and Fort Smith, located under the substorm auroral brightening, showed Pi2 pulsations near the time of auroral intensification as seen in Figures 2b and 2c. The B_Y (positive east) and B_Z (positive down) perturbations at Fort Simpson started at $\sim 0714:10$ UT (denoted by dashed vertical line in Figures 2b and 2c) at the same time as the perturbations of B_X (positive north) and B_Y at Fort Smith. Thus, 0714:10 UT is determined as the high-latitude Pi2 onset time.

[16] For midlatitude stations Ukiah, OR (magnetic latitude 51.317N, longitude 57.711W), Fort Yates, ND (mag. 55.756N, 35.281W), Remus, MI (mag. 54.647N, 12.992W) and Kapuskasing (mag. 60.183N, 8.605W) seen in Figures 2d–2g, the magnetic field perturbation (sudden increase or decrease in B_Y) started at 0713:38 UT (denoted by the vertical dashed line in Figures 2d–2g), which is chosen to be the midlatitude Pi2 onset time for this event.

[17] The location of the substorm current wedge (SCW) can be determined by the ground magnetic field B_Y at midlatitude stations Ukiah, Fort Yates, Remus, and Kapuskasing (from west to east geographically, Figure 2). After $\sim 0713:38$ UT (the midlatitude Pi2 onset time), all four stations (and many other stations, not shown here) observed gradual changes in B_Y . Until ~ 0716 UT, the overall change is positive at Ukiah and Fort Yates (and all stations west of Fort Yates), but negative at Remus and Kapuskasing (and all stations east of Kapuskasing). Therefore the SCW central meridian location is between Fort Yates and Remus.

[18] The substorm onset location from optical observations (determined to be on the eastern side of Fort Simpson

or at the coverage gap slightly to the east of the Fort Simpson ASI camera's field of view, seen in Figure S1 in Text S1) is to the west of the substorm meridian determined from ground magnetometers. Therefore, the auroral intensifications captured are located at the upward field aligned current region of the substorm current wedge.

[19] We project probes P1–P5 along magnetic field lines to the ionosphere using an event-dependent magnetic field model AM01 [Kubyskhina *et al.*, 2009] derived from a parameter search of the T96 [Tsyganenko, 1995] model but constrained to match THEMIS magnetic and plasma observations along the THEMIS meridian (see foot points in Figure 1a). The footprints of P1–P4 are all located near the SCW meridian (between Fort Yates and Remus); P5 is located in the view of Fort Smith, which captured the auroral intensification. As we will see in the next section, P3 and P4 observed intense magnetic field dipolarization and particle injections, whereas P5 did not observe significant changes. This implies either a possible mapping distortion in the MLT direction, such that P5, P3, P4 were further to the west by 1/2 in MLT, or an extremely thin flow channel responsible for the observed auroral signatures, confined to the meridian of the SCW where P3, P4 were fortuitously positioned. In either case, we infer from the mapping above and the ground signatures that at least the P3, P4 THEMIS satellites (and by inference P1 and P2 on the same meridian) were well positioned to examine the timing of substorm signatures in space. We note that P5 should have observed the substorm signatures in space given its position, barring small (but not unreasonable) mapping distortions and/or extreme localization of phenomena in space, which is an inherent supposition in our interpretation of the space signatures below.

3.2. Magnetotail Phenomena

[20] The positions of the THEMIS probes at ~ 0714 UT on 29 January 2008 are shown in Table 1. The five probes are aligned along the magnetotail, from $X_{GSM} = -7.8 R_E$ to $-29.5 R_E$ and within $4 R_E$ in the direction perpendicular to the nominal location of the neutral sheet, i.e., in a classical

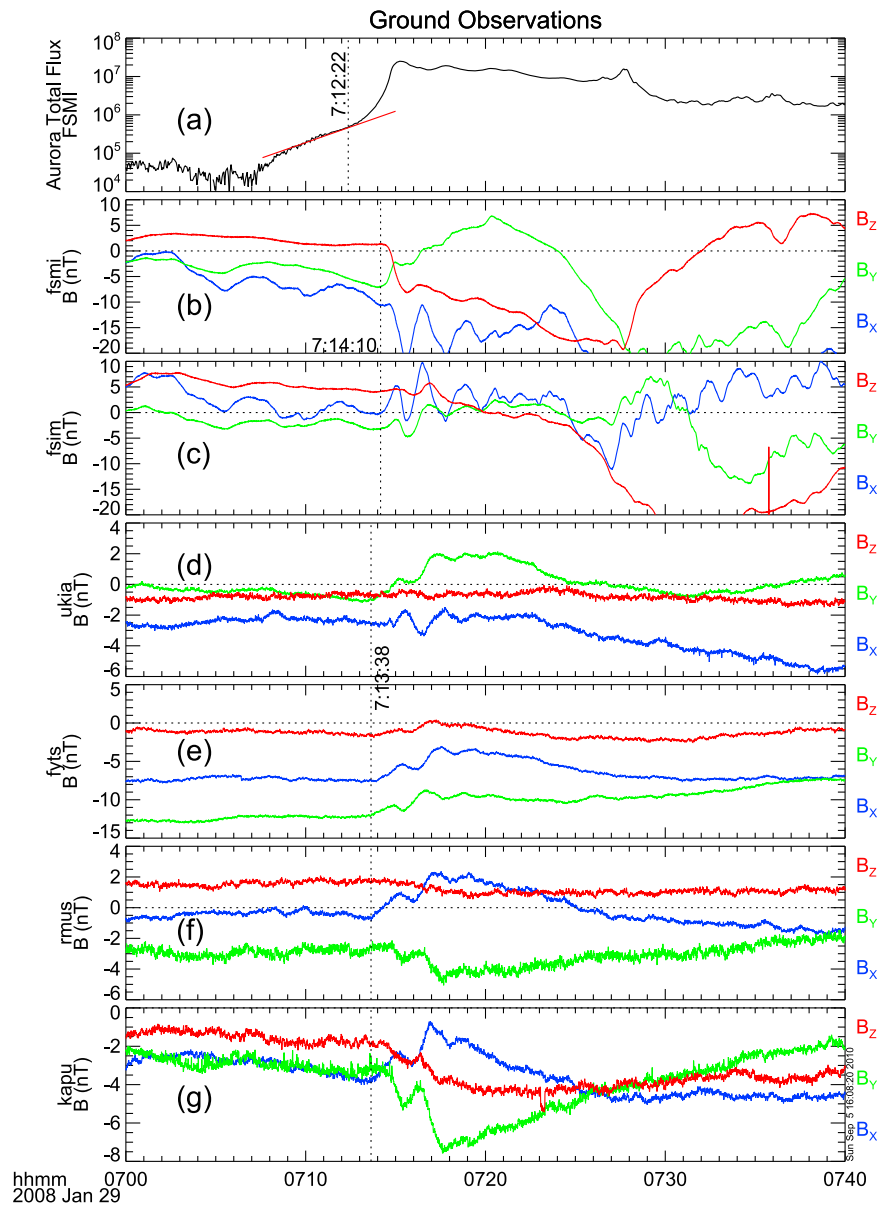


Figure 2. Ground magnetometer observations of geomagnetic and auroral activities for the 29 January event: (a) integrated light flux (rescaled) of the square in the Fort Smith all-sky image; geomagnetic observation (median removed) of high-latitude (b) Fort Smith and (c) Fort Simpson stations; and mid-latitude (d) Ukiah, (e) Fort Yates, (f) Remus, and (g) Kapuskasing stations (arranged from west to east on the map).

“major” THEMIS conjunction [Sibeck and Angelopoulos, 2008].

[21] At ~ 7 UT on 29 January 2009, the solar wind velocity had a persistent southward component of ~ 50 km/s, resulting in a 6.5° tilt of the magnetotail (Figure S3 in Text S1). Therefore, we rotate the GSM coordinate system clockwise about the Y_{GSM} coordinate to form a tilted GSM coordinate system, which is especially relevant for the more distant satellites, i.e., P1 and P2. For convenience, however, we plot all observations in this coordinate system.

[22] Several key observables from probes P1–P5 from 0700 UT to 0730 UT are shown in Figures 3 and 4, in the tilted GSM coordinate system. At the position of P1 ($X_{GSM} = -29.5 R_E$) and P2 ($X_{GSM} = -18.5 R_E$), the magnetic field B_x

component is stable, negative, and close to typical values near the plasma sheet boundary layer or lobe (Figures 3a and 3f). P3 and P4 observed a magnetic field with B_x

Table 1. Locations of the THEMIS Probes at ~ 0714 UT 29 January 2008^a

| Probe | X_{GSM} | Y_{GSM} | Z_{GSM} |
|-------|-----------|-----------|-----------|
| P1 | -29.5 | -0.73 | -9.22 |
| P2 | -18.5 | -1.4 | -6.01 |
| P3 | -11.0 | -2.13 | -3.74 |
| P4 | -10.8 | -1.17 | -3.74 |
| P5 | -7.88 | 1.71 | -2.55 |

^aIllustrated in Figure S2 in Text S1.

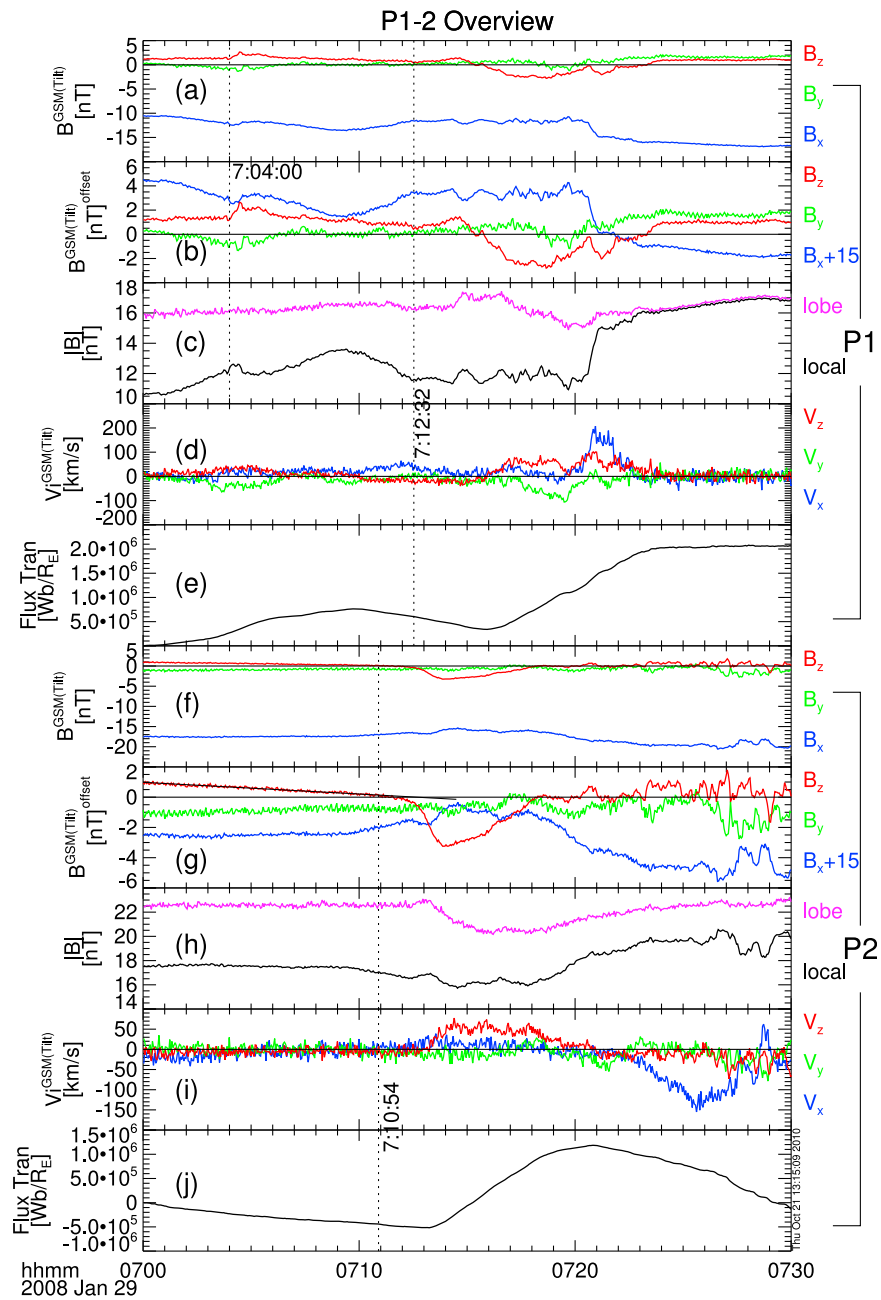


Figure 3. Overview plots of P1 and P2 for the 29 January event. There are five panels for each probe: (a, f) magnetic field, (b, g) magnetic field with B_x offset, (c, h) local magnetic field strength and lobe magnetic field strength (inferred from local measurements of total pressure), (d, i) low-energy (ESA) ion bulk velocity, and (e, j) cumulative magnetic flux transferred earthward and into the plasma sheet. Quantities are all in the tilted GSM coordinates.

and B_z components on the order of ~ 6 nT (Figures 4a and 4e). For P1–P4, the peak differential energy flux of ions is around 10keV, and the peak electron fluxes is at ~ 1 keV. The ion and electron flux at P3 and P4 are much higher than those at P1 and P2, however (see *Lui et al.* [2008] for details). Moreover, the magnetic field elevation on the inner probes was much higher than on the outer probes. Thus, P1–P4 were located inside the plasma sheet, but P3 and P4 were much closer to the neutral sheet than P1 and P2.

[23] Each of the five probes saw perturbations in the magnetic field. P1 observed a bipolar B_z signature (positive then negative) starting at 0712:32 UT (denoted by the vertical dashed line in Figures 3a–3e), consistent with a tailward moving nightside flux transfer event (NFTE) [*Sergeev et al.*, 1992]. Total pressure enhancement, one important attribute of NFTEs, was also observed at the center of the bipolar signature (Figure 3c, total pressure is represented as lobe magnetic field strength). This bipolar signature, indicating reconnection earthward of P1, cannot be revealed

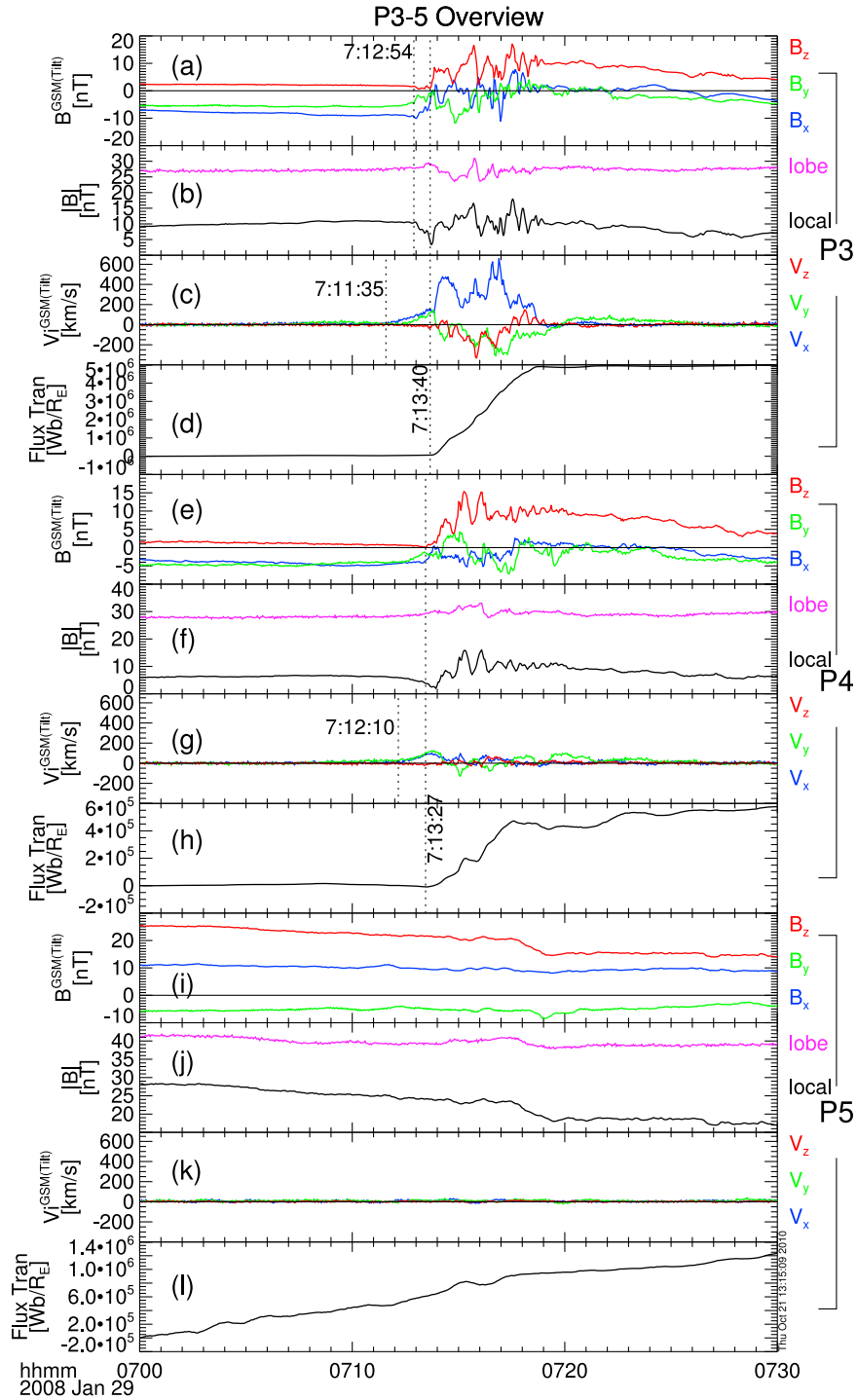


Figure 4. Overview plots of P3, P4, and P5 for the 29 January event. There are four panels for each probe: (a, e, i) magnetic field, (b, f, j) local magnetic field strength and lobe magnetic field strength (inferred from local measurements of total pressure), (c, g, k) low-energy (ESA) ion bulk velocity, and (d, h, l) cumulative magnetic flux transferred earthward and into the plasma sheet. All quantities are in the tilted GSM coordinates.

when plotting the data in the ordinary GSM coordinate system. Our working criterion of the first substorm signature for satellites located tailward of the reconnection site but outside the plasma sheet and observing a plasmoid is the first positive inflection point before the peak of the bipolar signature in B_z . In this case for P1, the first positive

inflection point before the peak of the bipolar signature is 0712:32 UT. P2 observed a negative B_z starting before 0712:32 UT (Figure 3g). But because of the continuing decreasing trend of B_z , presumably due to compression of the magnetic field and continued flaring, it is very difficult to determine accurately the time of the inflection point

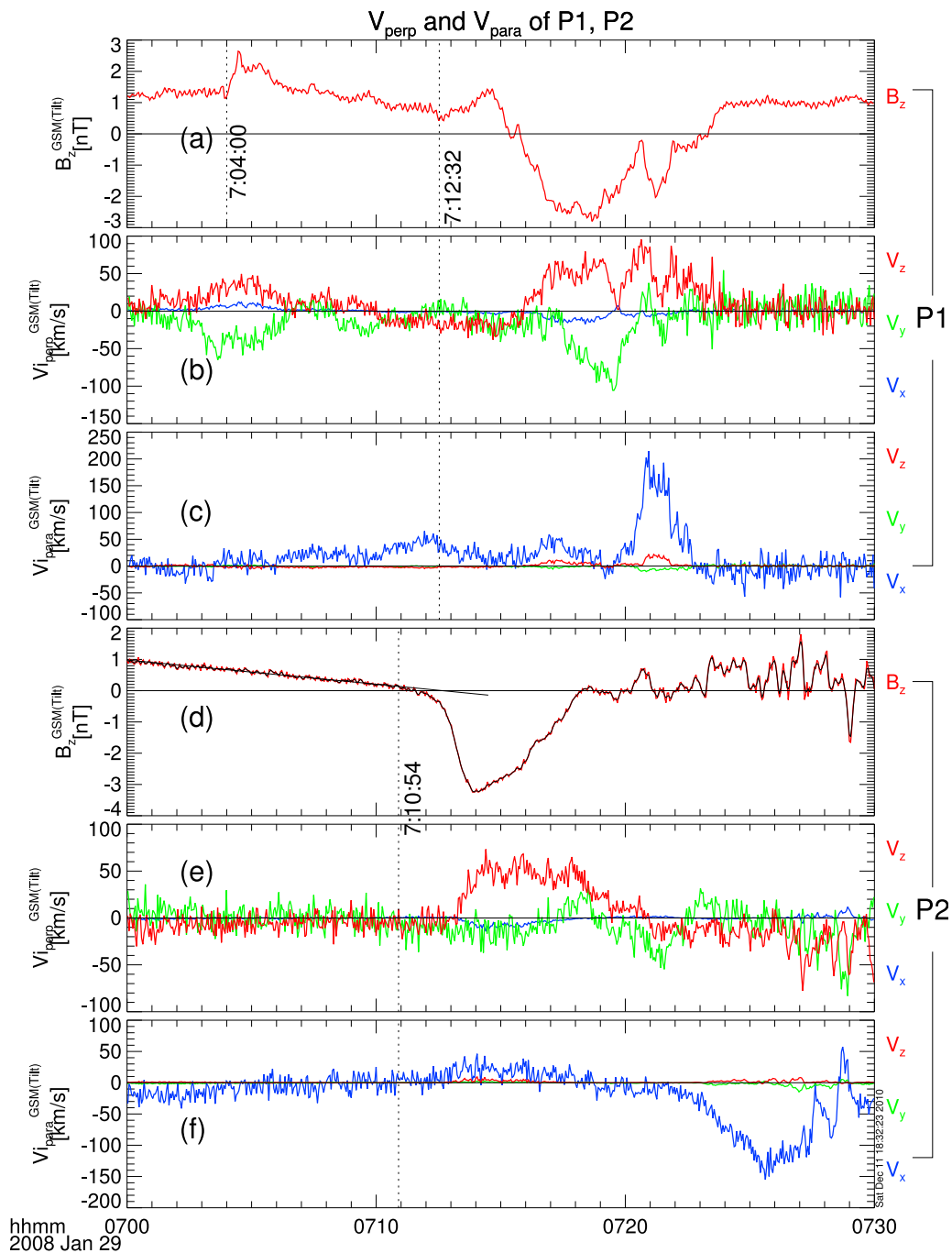


Figure 5. The 29 January event (three panels for each probe): (a, d) magnetic field z component and (b, e) perpendicular and (c, f) parallel (to the magnetic field) components of ion bulk velocity observed by P1 and P2. All quantities are in the tilted GSM coordinates.

signaling onset of reconnection topology underneath P2. In order to examine with greater fidelity the onset time at P2, we decompose the B_z variation into a slow linear decrease (a linear fit to the quiet time B_z decrease, shown in Figures 3g and 5d as a tilted thin black line) and a rapid change related to the emerging, exponentially growing reconnection topology. The inflection point is masked by noise in the original data (4 sample/s with a 2 Hz antialiasing low-pass filter) from the FGM data product utilized. We smoothed the original data with a 3-point boxcar average and superimposed the

smoothed data (thin black curve) on the original data (thick red curve) in Figure 5d. The deviation of the smoothed B_z from the linear fit of the quiet time measurement at 0710:54 UT is quite clear. We denote this inflection time in Figures 3f–3j and 5d–5f with a vertical dotted line. The southward inflection of the magnetic field on P2 indicates that the reconnection site was very close to and earthward of P2 (P2 was located at $X_{GSM} = -18.5 R_E$ at that time). P3 and P4 saw typical dipolarization signatures. The dipolarization on P3 started at 0713:40 UT, following a clear B_z perturbation at

0712:54 UT (Figure 4a). The dipolarization at P4, denoted by the vertical dashed line in Figures 4e–4h, happened at 0713:27 UT.

[24] An earlier magnetic activation at P1 (at 0704 UT) is evident in both Figures 3a–3c and 5a. A small, gradual increase in earthward flow was observed at that time and continued until primary onset. The origin and consequences of this activation are unclear. Because the activation was not observed at the other satellites, it is possible that it is simply a local preconditioning of the plasma sheet. However, the earthward flows could have extended all the way to the neutral sheet but have not been observed by P2 because it was farther away from the neutral sheet than P1. However, there is no evidence that these flows extended any farther or had any consequence in the near-Earth region. Thus, they are assumed to be only a localized activation at P1 and have no consequence for the global evolution. We therefore concentrate on the signatures around 0712 UT.

[25] The ion bulk flows observed at P1 and P2 at around 0712 UT demonstrate substorm onset-related signatures. P2 and P1 observed northward flows at ~0713 UT and ~0715 UT, respectively (Figures 3i and 3d) but did not record significant tailward flows because they were far away from the neutral sheet. Significant magnetic flux transport corresponding to the northward flows also began at ~0713 UT at P2 and at ~0715 UT at P1 (Figures 3j and 3e). The plasma flow and the magnetic flux transport (and also total pressure release, not shown) began considerably later than magnetic field inflection onset, by as much as several minutes, contrary to what is expected from satellites in the path of tail reconnection. One possible explanation is that the inflow, magnetic flux transport, and pressure reduction are significant enough to be seen far from the neutral sheet only when lobe reconnection takes off, depleting the lobe of its flux and reducing the cross-tail current, which happens significantly after the beginning of reconnection on closed plasma sheet field lines. In this explanation, the inflow generated by lobe reconnection could not reach P1 and P2 until several minutes after plasma sheet onset, and was most pronounced after the center of the plasmoid, which started to form by closed plasma sheet reconnection, had passed P2 and P1 (the negative portion of B_z) [e.g., Richardson and Cowley, 1985; Angelopoulos *et al.*, 2008b, 2009], at ~0713 UT and ~0715 UT, respectively. Lui *et al.* [2008] chose ~0713 UT as the onset time at P2 based on the inflow onset time, whereas we interpret the magnetic field B_z inflection at 0710:54 UT as the onset time on P2, which is the direct consequence of plasma sheet reconnection.

[26] P3 observed a strong earthward flow with a peak value of ~600 km/s; P4 saw an earthward flow of ~100 km/s. Energetic particle injections were observed by both P3 (see 100–300 keV energies in Figure 6 of Lui *et al.* [2008]) and P4 (not shown but available on the THEMIS website). The injections and the dipolarization occurred simultaneously. Note, however, in Figures 4a and 4c and Figures 4e and 4g that the earthward flow at P3 and P4 started much earlier than the dipolarizations at those probes; even earlier than any substorm-related signatures in the tail and the auroral intensification. This fact may lead to the speculation that the substorm initiated somewhere near P3 and P4. Meanwhile, P1 also observed an earthward flow burst of ~150 km/s at

~0720 UT, which contradicts the interpretation that the reconnection site was earthward of P1.

[27] To investigate the true nature of the ion flows, we split the ion flow into components perpendicular and parallel to the magnetic field. The perpendicular and parallel components of the ion bulk velocity from P1–P4 are shown in Figures 5 and 6, along with the magnetic field z component (the calculation of the perpendicular and parallel flow to the magnetic field is point to point). At P1 and P2, perpendicular flows were northward ($V_z > 0$, peak 50 km/s) when the B_z perturbation was negative (Figures 5a, 5b, 5d, and 5e). These flows were interpreted in the previous paragraphs as the inflow toward the neutral sheet, generated by lobe reconnection after the plasmoid had passed the probe. Figures 6c and 6f shows that the earliest earthward flow at P3 (0711:35 UT) and P4 (0712:10 UT) are field-aligned flows, while the convection flow (perpendicular flow) occurred at the same time as the dipolarization (Figures 6a, 6b, 6d, and 6e). The early enhancement of the parallel flow can be explained as due to the pressure imbalance caused by plasma sheet thinning before substorm initiation [Birn and Schindler, 1985]. Some of the flow, however, may be due to ion acceleration ahead of the dipolarization front [Zhou *et al.*, 2010] or diversion of the flow ahead of the front by the curvature forces exerted by the front. The perpendicular flows are signatures directly related to the arrival of the front itself. This interpretation can be further confirmed by the enhancement of the cumulative magnetic flux transport at the same time (Figures 4d and 4h). Note that the exact time of onset of parallel flow at P4 (determined at 0712:10 UT) does not affect the results herein.

[28] Finally, the earthward flows at P1 are field aligned (Figure 5c). Detailed examination of the ion distribution functions (Figure S4 in Text S1) shows that the dominant field-aligned flow results from an imbalance between counterstreaming beams at the plasma sheet boundary, with the earthward beam having higher speed and density than the tailward beam. This behavior is expected from distant tail reconnection [DeCoster and Frank, 1979; Takahashi and Hones, 1988]. Parallel flows are likely the result of reconnection in the distant tail; perpendicular flows are caused by local plasma sheet convection. Another interesting observation is that V_y is comparable to V_x at P4 for both parallel and perpendicular flows. Interpreted as slant crossing of the flows arriving from the tail, this observation suggests that azimuthal propagation should also be considered when doing substorm timing of localized reconnection phenomena, which are likely more akin to reconnection points than reconnection lines.

[29] In summary, our observations suggest that whereas distant tail reconnection was ongoing, midtail reconnection onset took place prior to 0712:32 UT, between P1 and P3, and (based on the southward B_z turning at P2) most likely earthward of P2. A summary of the timing of these phenomena will be presented in section 5.

4. The 2 February 2008 Event

[30] The substorm event on 2 February 2008 was studied in detail by Mende *et al.* [2009]. It consists of three successive substorms: one at ~0740 UT, one at ~0812 UT, and one at

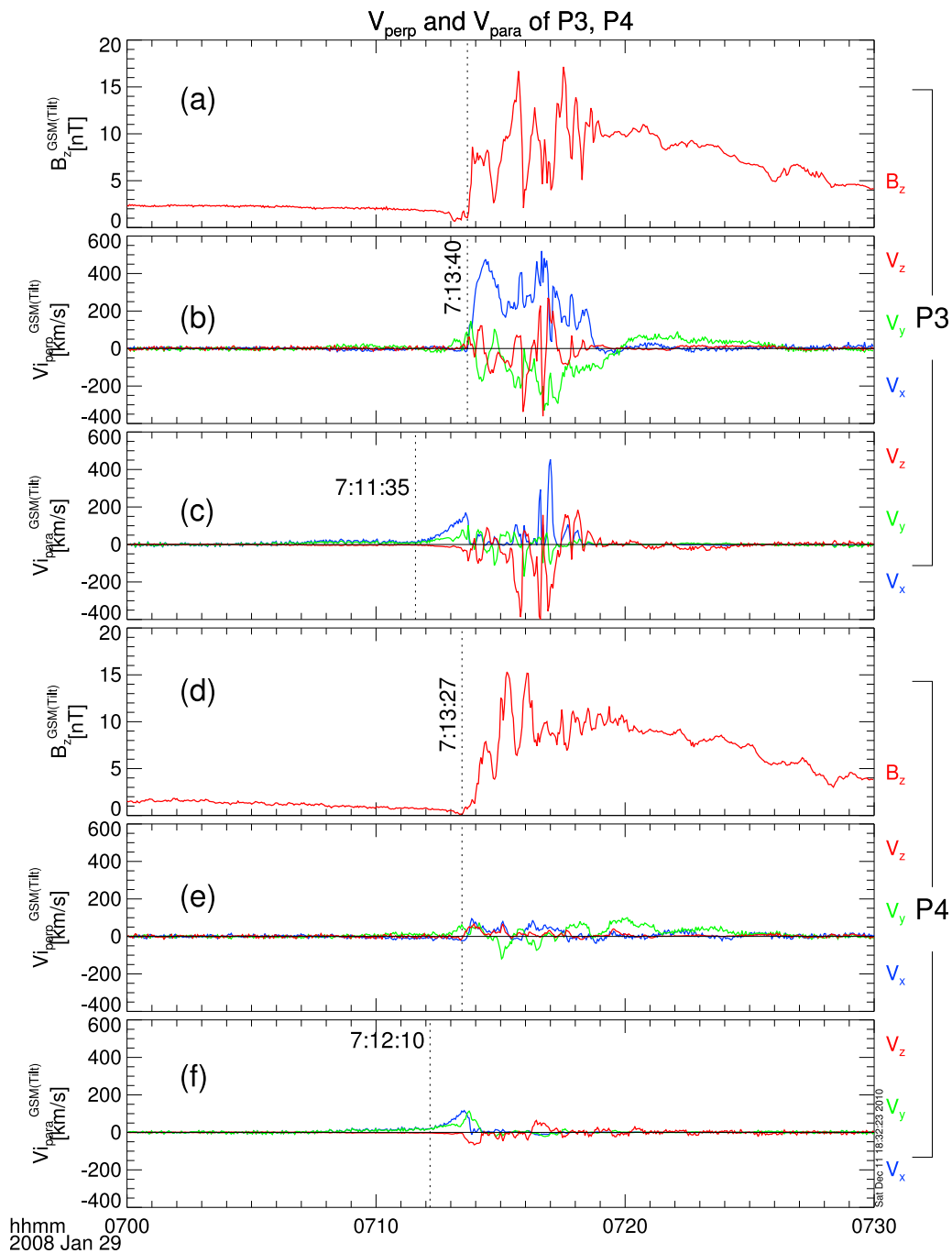


Figure 6. The 29 January event (three panels for each probe): (a, d) magnetic field z component and (b, e) perpendicular and (c, f) parallel (to the magnetic field) components of ion bulk velocity observed by P3 and P4. All quantities are in the tilted GSM coordinates.

~0835 UT. Here we only consider the first substorm at ~0740 UT. We first briefly describe the timing results of this event and introduce a slightly revised timing at P1 relative to *Mende et al.* [2009]. A summary of all timing signatures is presented in section 5.

[31] Auroral activities were captured in the fields of view of Gillam, Fort Smith, and Fort Simpson, as shown in Figure 7. In Figure 7a we also mark the footprints of the five THEMIS probes using the event-based magnetic field model AM01 [*Kubyshkina et al.*, 2009]. Auroral intensification occurs

at ~0738:55 UT, and poleward expansion occurs at ~0741:00 UT (This is in agreement with the onset determinations of *Mende et al.* [2009, Figures 6 and 7]). Several ground-based magnetometers observed geomagnetic field perturbations related to the substorm event. The high-latitude Pi2 onset started at ~0739:05 UT, and the midlatitude Pi2 onset was determined to begin at ~0741:05 UT (Figure S6 in Text S1).

[32] The positions of the THEMIS probes at ~0740 UT on 2 February 2008 are shown in Table 2. The observations

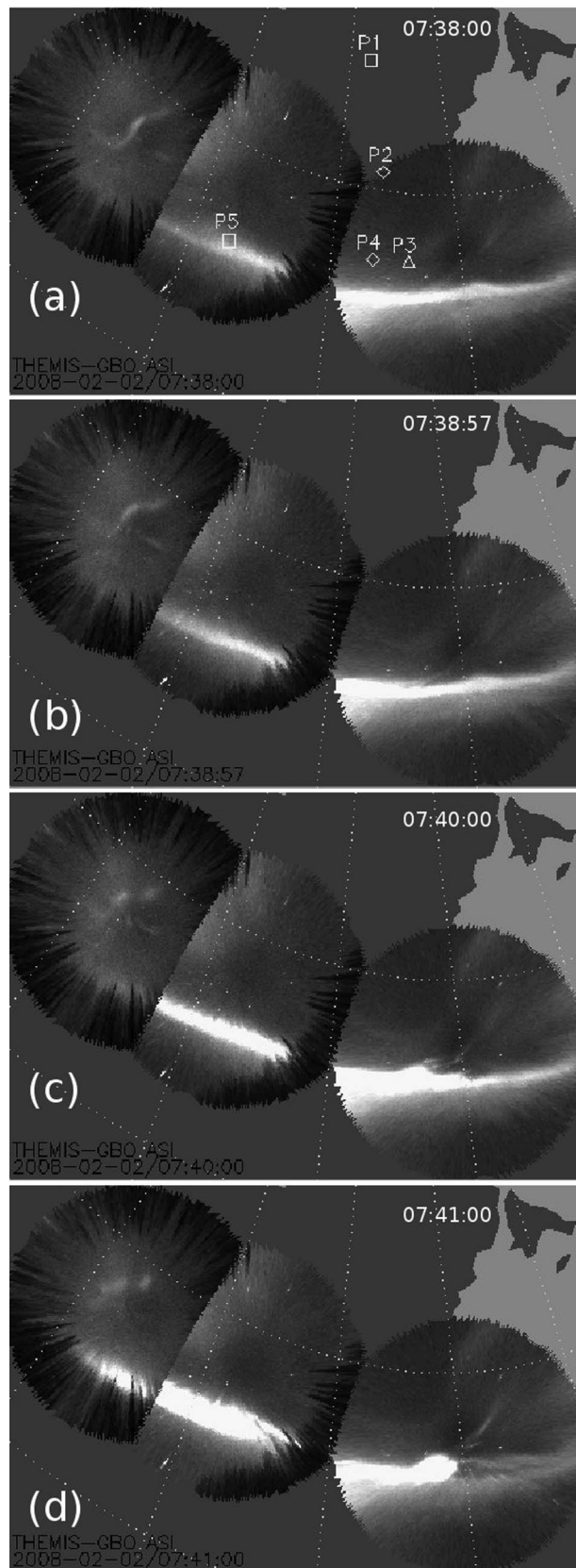


Figure 7. All-sky imagers' aurora photographs of the 2 February event at (from west to east) Fort Simpson, Fort Smith, and Gillam.

from the outermost probe, P1, ($X_{GSM} = -29.7 R_E$) and innermost probe, P5 ($X_{GSM} = -8.3 R_E$), are shown in Figure 8. There is a distinguishable bipolar (positive then negative) B_z signature in P1's magnetic field observations (Figure 8a). We interpret this B_z bipolar signature as caused by a tailward moving plasmoid or NFTE generated by a reconnection event earthward of P1. The total pressure peak (Figure 8b, represented as lobe magnetic field strength) around the center of the bipolar B_z signature, which is a typical phenomenon produced by traveling NFTEs, confirms this interpretation. Using the same criteria as in the previous event, that the first positive inflection point before the peak of the bipolar signature in B_z marking the plasmoid arrival is the first signature of plasma sheet reconnection at a probe near the plasma sheet boundary tailward of the reconnection site, we select the onset time at P1 to be 0737:35 UT. This time is denoted by a vertical dashed line across the P1 panels in Figure 8. As for the earlier event examined, there is some indication of a local precursor signature in the B_z component of the magnetic field at 0732:40 UT (marked by a vertical dashed line) but no evidence of other activity either locally on P1 or at the inner probes. Since there were no flows inward (toward the neutral sheet) at P1 were associated with this deflection, we take this to be only a minor activation or flapping, with no global effects. The role of the dominant bipolar signature at 0737:36 UT as evidence of a reconnection onset is also confirmed by the negative inflection of the cumulative magnetic flux transport at the same time (Figure 8e). The B_z positive inflection time may also be put at 0738:30 UT or 0740:00 UT, as is marked by two arrows in Figure 8a, but the cumulative magnetic flux transport (Figure 8e) did not show negative deflection at these two points. The negative deflection of cumulative magnetic flux transport is a significant indicator of the plasmoid leading edge [Liu *et al.*, 2011], so 0737:36 UT is better qualified as the arrival time of the plasmoid than 0738:30 UT and 0740:00 UT. As with the 29 January 2008 substorm, P1 was not close enough to the neutral sheet to capture significant tailward flows. However, the presence of lobeward ($V_z < 0$) then equatorward ($V_z > 0$) flows accompanied by the northward ($B_z > 0$) then southward ($B_z < 0$) deflection of the field is consistent with the tailward motion of a TCR equatorward of the probe, presumably produced by reconnection earthward of P1. Lack of observations from P2, due to a NASA ground station overwrite of the data on that day, prohibits corroborative evidence of the reconnection process from P2.

[33] The innermost satellite, P5, observed earthward flows at $\sim 0739:10$ UT (Figure 8h) and dipolarization at $\sim 0740:00$ UT (Figure 8f), indicating that P5 was earthward

Table 2. Locations of the THEMIS Probes at ~ 0745 UT 2 February 2008^a

| Probe | X_{GSM} | Y_{GSM} | Z_{GSM} |
|-------|-----------|-----------|-----------|
| P1 | -29.7 | 0.104 | -8.76 |
| P2 | -18.5 | -0.885 | -5.76 |
| P3 | -11.1 | -1.883 | -3.60 |
| P4 | -11.1 | -0.956 | -3.66 |
| P5 | -8.34 | 1.71 | -2.709 |

^aIllustrated in Figure S5 in Text S1.

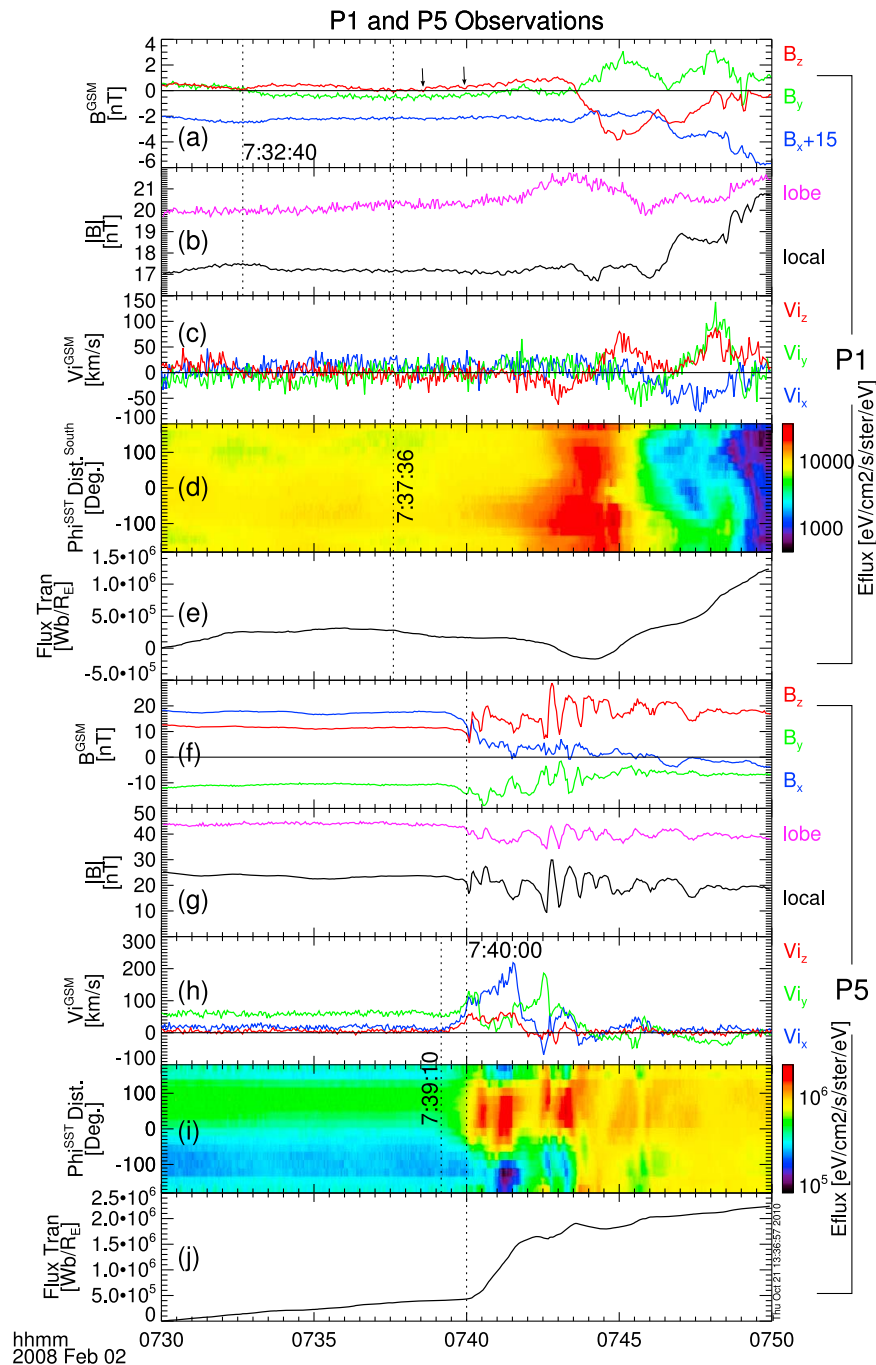


Figure 8. Overview plots of P1 and P5 for the 2 February event. There are four panels for each probe: (a, f) magnetic field, (b, g) local magnetic field strength and lobe magnetic field strength (inferred from total pressure local measurements), (c, h) low-energy (ESA) ion bulk velocity, (d, i) ESA ion Phi-Eflux distribution (only southward particles for P1), and (e, j) cumulative magnetic flux transport. Quantities are in GSM coordinates.

of the reconnection site. The earthward flows at P5 are all convective flows. Thus, the earliest substorm-related signature at P5 was the earthward flow onset. Although dipolarization at P3 and P4 ($X \sim -10 R_E$) occurred at $\sim 0740:54$ UT and $\sim 0741:20$ UT, respectively (Figure S7 in Text S1), there were magnetic field oscillations previous to these dipolarizations. The magnetic field precursor waves at P3 and P4

were at $\sim 0738:34$ UT and ~ 0739 UT, respectively, earlier than any signature at P5. P3 and P4 were far away from the neutral sheet near the plasma sheet boundary layer ($B_x \sim -40$ nT), so the magnetic precursor waves may be caused by the field-aligned electrons near the boundary layer. The magnetic field precursor waves at P3 were not accompanied by earthward flows, and the cumulative magnetic flux

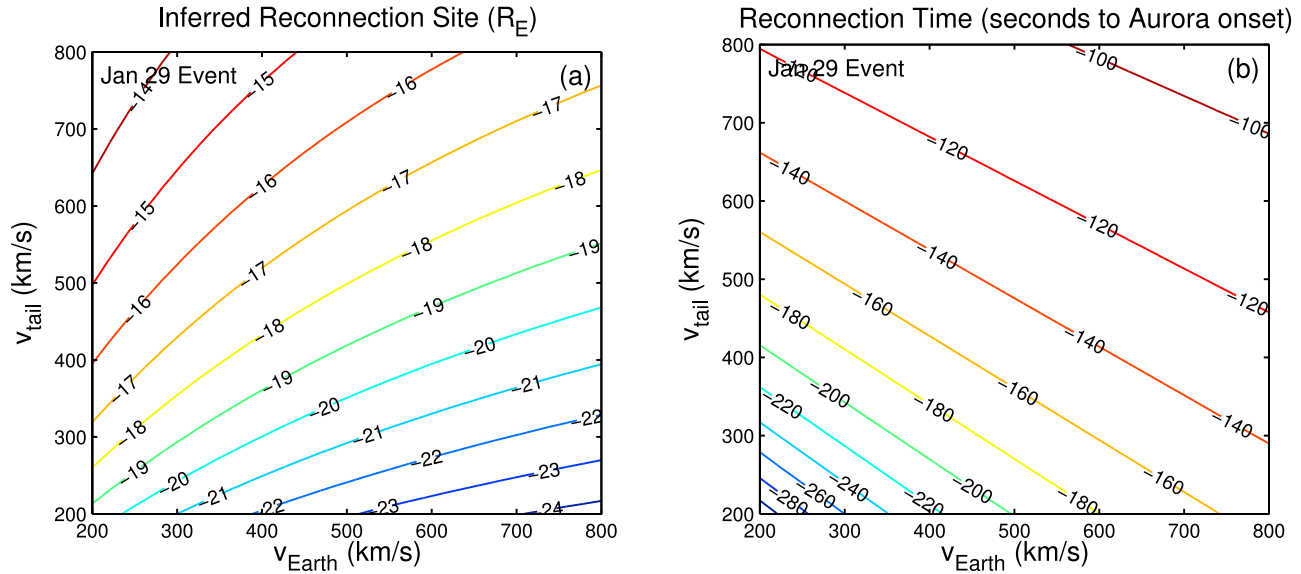


Figure 9. Possible reconnection (a) site and (b) time of the ~ 0713 UT 29 January event as a function of possible earthward and tailward magnetosonic speed V_{Earth} and V_{Tail} , based on the timing results at P1 and P4.

transport at P3 did not begin to increase until $\sim 0741:52$ UT, indicating earthward flux transport onset at that time. Unfortunately, P4 didn't have ESA coverage. In all, it is clear from this discussion and the data seen in the auxiliary material that P5 had the earliest signatures of substorm onset in the inner magnetosphere, and we therefore use those to perform substorm onset localization and timing analysis.

5. Reconnection Site Determination

[34] Seeking the onset of the substorm instability in the magnetotail, we use the first signature of substorm phenomena at each probe to determine activation location and onset time. Based on observations of P1 on one side and P3–P5 on the other side of the reconnection site, we can determine the onset location and time of that process.

[35] The magnetosonic speed (V_{MS}) in the central plasma sheet is expressed as $V_{MS}^2 = V_{th}^2 + V_A^2$, where V_{th} is the thermal speed ($V_{th}^2 = p/\rho$), and V_A is the Alfvén speed ($V_A^2 = B^2/\mu_0\rho$). Typical plasma parameters near the neutral sheet around $10 R_E$ down tail ($|B| \sim 3$ nT, $n \sim 0.5$ /cc, $T \sim 3$ keV) yield V_{MS} of ~ 550 km/s with V_{th} of ~ 540 km/s and V_A of ~ 90 km/s. From $10 R_E$ to $30 R_E$ down tail the magnetic field strength and particle density remain relatively unchanged. Thus, magnetosonic speed variation depends mainly on the variation in temperature. Statistical studies of plasma sheet temperature [Wang *et al.*, 2004] suggest that the temperature changes by at least a factor of 2 from $10 R_E$ to $20 R_E$ down tail, and thus the thermal speed can differ by at least 40% between the two sides of the reconnection site. This suggests the importance of using different (independent) average propagation speeds on the two sides of the reconnection site and constraining either one separately by local measurements, if available. Thus, contrary to the hypothesis of a constant propagation speed on both sides of the reconnection site (the magnetosonic speed in the plasma sheet) used

by Angelopoulos *et al.* [2008b] and Liu *et al.* [2009], and in particular for the 0740 UT 2 February 2008 event in the work by Mende *et al.* [2009], here we assume that the earthward and tailward propagation speeds on the two sides can be different. The reason for this generalization of the timing analysis is that the distance between P1 and the inner probes in this particular case is so large ($\sim 20 R_E$) that the hypothesis of a constant magnetosonic speed seems quite unrealistic. Under this assumption, the reconnection site x_r (GSM) and reconnection time t_r can be obtained by solving the following 1-D, simplified equations:

$$x_E - x_r = V_{\text{Earth}}(t_E - t_r), \quad (1)$$

$$x_r - x_t = V_{\text{Tail}}(t_t - t_r), \quad (2)$$

where x_E and x_t are the positions of the probe earthward of the reconnection site and the probe tailward of the reconnection sites respectively; t_E and t_t are the time when these two probes saw the earliest signature related to the substorm; and V_{Earth} and V_{Tail} are the average magnetosonic speed earthward and tailward of the reconnection sites, respectively. The average magnetosonic speed on both sides is expected to be between 200 km/s and 800 km/s based on typical values of the field and plasma parameters at those locations. We can then solve the equations for the reconnection site x_r and reconnection time t_r as a function of V_{Tail} and V_{Earth} with the simplification that the substorm propagates one-dimensionally parallel to the X_{GSM} axis.

[36] For the 29 January event, we use the NFTE onset at P1 as the first tailward propagation signature of the substorm ($x_t = -29.5 R_E$, $t_t = 0712:32$ UT) and the earthward flow onset at P3 as the earthward propagation signature ($x_E = -10.8 R_E$, $t_E = 0711:35$ UT). This is justified by the reconnection signatures at P2, and that P2 was observed to be very close to the reconnection site (given the large inflow toward

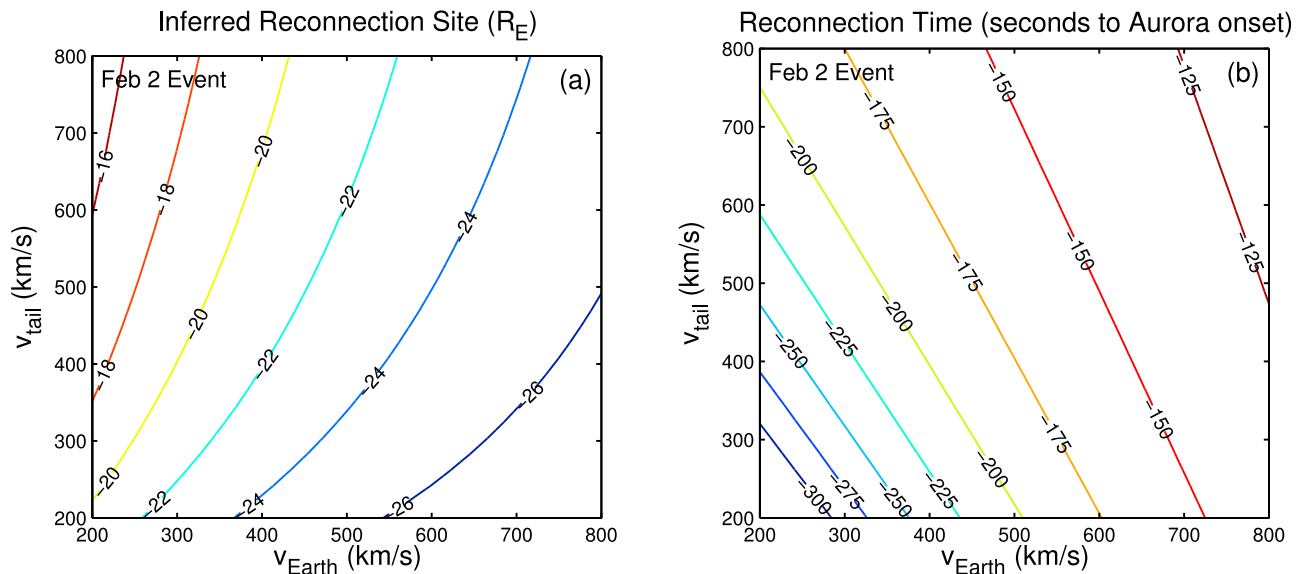


Figure 10. Possible reconnection (a) site and (b) time of the ~ 0740 UT 2 February event as a function of possible earthward and tailward magnetosonic speed V_{Earth} and V_{tail} , based on the timing results at P1 and P5.

the plasma sheet observed in the V_z component of the flow). The site and time of reconnection determined with this input is shown in Figure 9. When the tailward propagation speed is 440–540 km/s and earthward propagation speed is 520–620 km/s (consistent with the measured magnetosonic speed of ~ 570 km/s at P4, the closest probe to the neutral sheet at $\sim 10 R_E$), the resultant reconnection site can be around $18.5 \pm 0.7 R_E$, at, or just earthward of P2, consistent with the magnetic and flow signatures at P2. The corresponding reconnection time can vary from $\sim 0710:00$ UT to $\sim 0710:20$ UT. The exact location may not only be uncertain to within $\sim 2 R_E$ based on uncertainty in the magnetosonic speed, but also it can be extended by several R_E along the tail, and may move around in response to interaction with the earthward plasma. This is something to be analyzed in the future using events with probes positioned closer to the neutral sheet. The inferred reconnection time (0710:00–0710:20 UT) may seem to disagree with the magnetic field inflection time at P2 (0710:54 UT). P2 was very close to the inferred reconnection site in X direction, and one would think that it should have felt the effect of reconnection almost instantly. We interpret the delayed response at P2 as due to its position relative to the reconnection site, the reconnection geometry, and the plasmoid topology. First, there is always a possibility that the X point was displaced in the Y direction from the probe (P2 $Y_{\text{GSM}} = -1.4 R_E$, while substorms often happen in the premidnight sector); and clearly, P2 is displaced in the Z direction from the neutral sheet (regardless of GSM coordinates) as its measured B_x is around -20 nT. If we assume P2 to be $4 R_E$ away from the initial reconnection site, it takes ~ 40 s for the fastest signal to reach P2 from that site (the measured magnetosonic speed at P2 is 670 km/s). Meanwhile, the reconnection region could be very long. The longer the reconnection region (in the X direction) is, the less of an inclination change the magnetic field will undergo at onset. If P2 is exactly below the X line, which remains

steady, there would be no magnetic field inclination change until the plasmoid has been fully formed and expanded to divert the field at the P2 location, which may be a very slow process. Therefore, a possible explanation of the delayed response at P2 is that the initial reconnection event did not change the direction of the field immediately, as it takes time for the plasmoid to rotate the field topology at P2 and for the reconnection inflow region to expand to P2.

[37] For the 2 February event, we use the NFTE onset at P1 as the tailward event ($x_t = -29.7 R_E$, $t_t = 0737:36$ UT) and the earthward flow onset at P5 as the earthward event ($x_E = -10.8 R_E$, $t_E = 0739:10$ UT). The site and time of reconnection determined with this input are shown in Figure 10. The most likely location of the reconnection site for typical values of magnetosonic speeds of $V_{\text{Earth}} \sim 450$ – 650 km/s and $V_{\text{tail}} \sim 350$ – 500 km/s is $X \sim -22$ to $-25.5 R_E$; and the larger the ratio of V_{Earth} to V_{tail} , the further down the tail the reconnection site is. The assumption that the earthward propagation speed is larger than the tailward propagation speed is reasonable, since the magnetic field, density, and temperature earthward of the reconnection site are larger than tailward of the reconnection site. The corresponding reconnection time can vary from $\sim 0733:40$ UT to $\sim 0736:40$ UT. We note, that the measured magnetosonic speed at P5 is ~ 790 km/s, but P5 is far away from the neutral sheet ($|B| = \sim 23$ nT). Therefore, we cannot use this measurement to estimate the magnetosonic speed deep inside the plasma sheet as we did for the 29 January event. Alternatively, if we use the 0738:30 UT or 0740:00 UT (the two arrows in Figure 8a) as the NFTE onset time at P1, the inferred reconnection sites will be 2 – $4 R_E$ closer to Earth (but are still around $\sim 20 R_E$ down tail with reasonable V_{Earth} and V_{tail} assumptions) and the inferred reconnection time will be earlier by 20–50 s.

[38] After simple manipulations of equations (1) and (2), we can get the derivatives of V_{tail} as a function of V_{Earth}

Table 3. Timeline of the ~0713 UT 29 January Substorm Event^a

| Event | Time (UT) | $X_{GSM} (R_E)$ |
|----------------------------|----------------|-----------------|
| Tail reconnection | 0710:10 ± 10 s | -17.8~-18.5 |
| B_z inflection at P2 | 0710:54 | -18.5 |
| Earthward V_{par} at P3 | 0711:35 | -11.0 |
| Earthward V_{par} at P4 | 0712:10 | -10.8 |
| Aurora intensification | 0712:12 | -1 |
| NFTE at P1 | 0712:32 | -29.5 |
| Earthward V_{perp} on P4 | 0713:27 | -10.8 |
| Dipolarization on P4 | 07:13:27 | -10.8 |
| Midlatitude Pi2 | 0713:38 | -1 |
| Earthward V_{perp} on P3 | 0713:40 | -11.0 |
| Dipolarization on P3 | 0713:40 | -11.0 |
| High-latitude Pi2 | 0713:38 | -1 |

^aIllustrated in Figure 11.

when the reconnection site (x_r) or reconnection time (t_r) are fixed:

$$\frac{dV_{tail}}{dV_{Earth}} = \frac{(x_E - x_t)(t_t - t_E)V_{Earth} + (x_r - x_t)(x_E - x_r)}{[(t_t - t_E)V_{Earth} + x_E - x_r]^2}, \quad (3)$$

$$\frac{dV_{tail}}{dV_{Earth}} = -\frac{t_E - t_r}{t_t - t_r}, \quad (4)$$

$$\frac{d^2V_{tail}}{dV_{Earth}^2} = \frac{2(x_r - x_t)(x_E - x_r)(t_E - t_t)}{[(t_t - t_E)V_{Earth} + x_E - x_r]^3}. \quad (5)$$

[39] These equations can help us understand the shapes of the contours in Figures 9 and 10. The denominator of the right part of equation (3) being always positive, the outlines of the contours in Figures 9a and 10a depend on its numerator. For the 29 January event the Earth side onset time is earlier than the tail side onset time, making the numerator always positive. For the 2 February event, though the Earth side onset time is later than the tail side, making the first term of the numerator negative, the numerator remains positive for the V_{Earth} range of 200~800 km/s. Therefore, the contours in Figures 9a and 10a are both monotonically increasing functions of V_{Earth} . Similarly, for equation (5) we find that d^2V_{tail}/dV_{Earth}^2 is always negative for the 29 January event and remains positive (when V_{Earth} is 200~800 km/s) for the 2 February event. This explains the shape of the curves in Figures 9a and 10a. Equation (4) predicts that all the contours in Figures 9b and 10b are monotonic with negative slope. The slope is bigger than -1 when the Earth side onset time is earlier than the tail side onset time as in the 29 January event (Figure 9b), and it is smaller than -1 when the Earth side onset time is later than the tail side onset time as in the 2 February event (Figure 10b).

6. Discussion and Conclusions

[40] After determining the reconnection site and time, we list the time lines of the two substorm events in Tables 3 and 4, and illustrate them in Figures 11 and 12. The inferred reconnection onset time for both events is slightly earlier than any observable substorm onset signatures in space or on the ground.

[41] Our timing of these events differs from previous studies mainly in the timing and interpretation of the magnetotail signatures. On the ~0714 UT 29 January event, *Lui et al.* [2008] timed the onset at P2 to be ~0713 UT (the equatorward flow onset time) and on that basis concluded that various substorm activities at P3 were earlier than those at P2, indicating that the initiation of the substorm is closer to P3 than P2. *Lui et al.* [2008] also argued that the southward dipping of the magnetic field and earthward plasma flow (parallel to the magnetic field) observed by P1 were due to plasma sheet thinning and crossing of the plasma sheet boundary layer. Indeed, at first glance these signatures appear inconsistent with magnetic reconnection occurring earthward of P1. However, after recognizing that the solar wind velocity would have caused a significant rotation of the plasma sheet, we have reinterpreted the P1 magnetic field signature in the inclined plasma sheet frame as the bipolar signature of a tailward moving plasmoid. Close examination of the ion distribution functions reveals that the observed earthward flow was due to counterstreaming beams, which suggests that the flow could be explained by distant-tail reconnection and is irrelevant to the near-Earth reconnection picture. The convective flow of the plasma, however, was found to be consistent with zero, or slightly tailward. The new observations reopened the question of the signatures at P2 as due to the reconnection topology that started to take shape significantly before the inflow of lobe plasma toward the plasma sheet. We then performed timing of the reconnection onset assuming different propagation speeds on the two sides of the reconnection site, using the timing signatures at P1 and P4. We obtained a reconnection onset time that is in agreement with the signatures of P2, if reasonable delays due to P2's vertical or possible azimuthal distance from the reconnection site are further considered. We also find that the early flow enhancement at P3 (0711:35 UT) as well as at P4 (0712:10 UT) is consistent with remote signatures of an approaching dipolarization front and that the time of dipolarization front arrival and magnetic flux transport was later than the first signature at either P2 or P1. While the THEMIS probe alignment for this event is not optimal, the interpretation of the signatures is consistent with tail reconnection initiation of substorm onset. For the auroral intensification time we picked 0712:22 UT, also different from the time of *Lui et al.* [2008] (~0714 UT), but even if we were to use the *Lui et al.* [2008] auroral onset

Table 4. Timeline of the ~0740 UT 2 February Substorm Event^a

| Event | Time(UT) | $X_{GSM} (R_E)$ |
|---------------------------|----------------|-----------------|
| Tail reconnection | 0735:10 ± 90 s | -22~-25.5 |
| NFTE at P1 | 0737:36 | -29.7 |
| Magnetic precursor at P3 | 0738:04 | -11.1 |
| Aurora intensification | 0738:55 | -1 |
| High-latitude Pi2 | 0739:05 | -1 |
| Earthward flow at P5 | 0739:10 | -8.5 |
| Dipolarization at P5 | 0740:00 | -8.5 |
| Dipolarization at P3 | 0740:54 | -11.1 |
| Aurora poleward expansion | 0741:00 | -1 |
| Midlatitude Pi2 | 0741:05 | -1 |
| Dipolarization at P4 | 0741:20 | -11.1 |
| Flux transport at P3 | 0741:52 | -11.1 |

^aIllustrated in Figure 12.

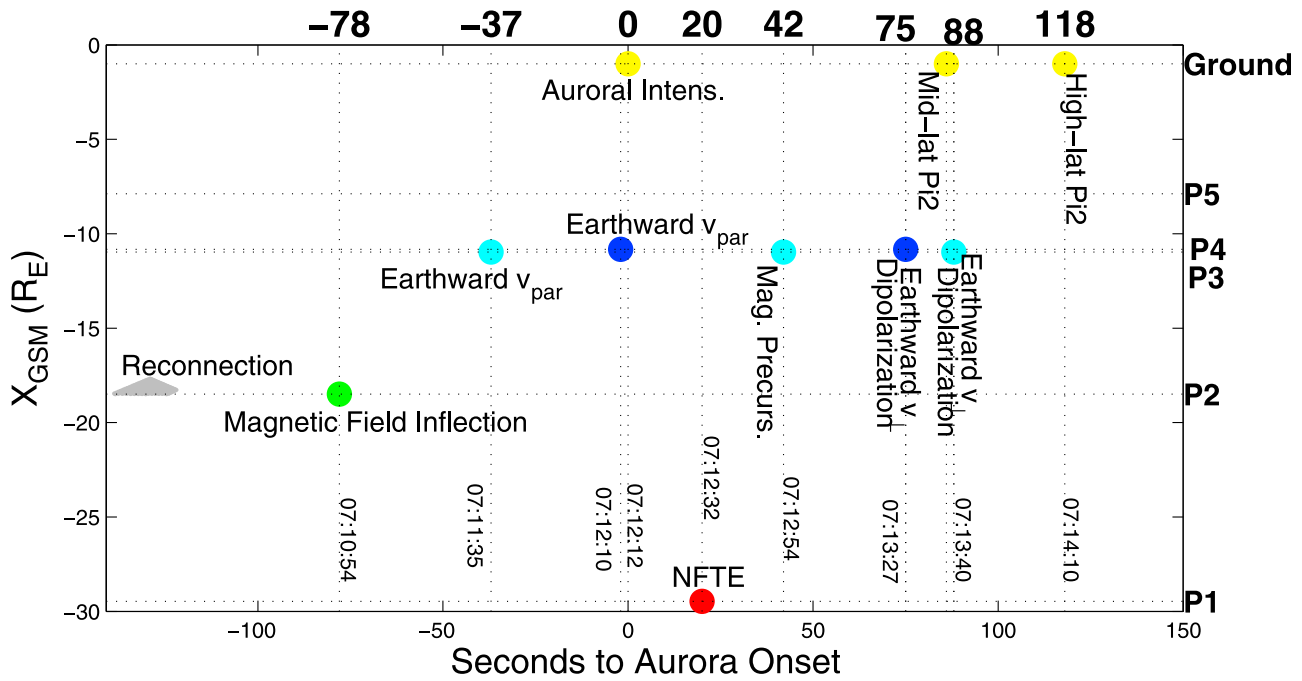


Figure 11. The location and time (seconds relative to auroral onset) of the events related to the ~0713 UT 29 January substorm. Colors represent different probes: red, P1; green, P2; cyan, P3; blue, P4; magenta, P5; yellow, ground observatories. The gray area represents the inferred possible reconnection site and time.

selection, the reconnection-triggered onset interpretation for this substorm event still stands well (if not better).

[42] For the ~0740 UT 2 February event, the major difference from *Mende et al.* [2009] is that the start of the plasmoid appearance at P1 is selected to be 0737:35 UT

instead of 0743:39 UT. We note that this event is also less opportune than other THEMIS conjunctions, due to the great distance of P1 from the neutral sheet as well as the lack of data from P2. The new timing of the P1 signatures, combined with the hypothesis of a different propagation

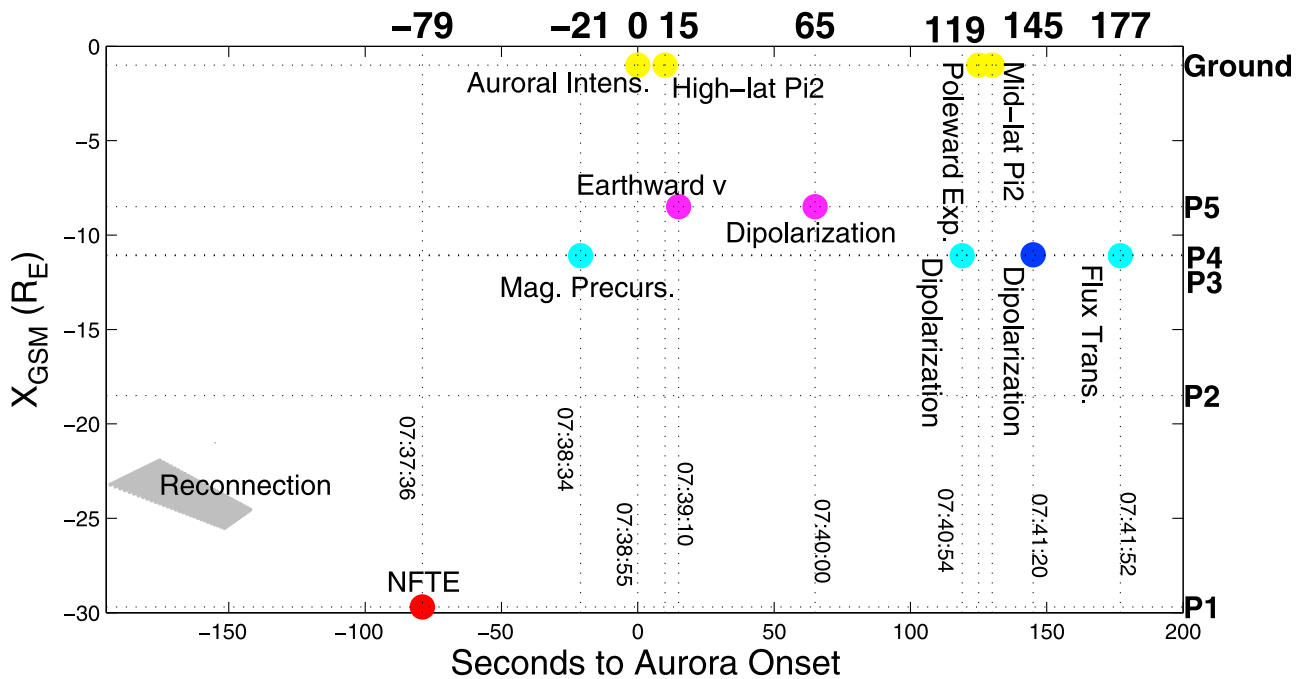


Figure 12. Same as Figure 11 but for the ~07:40 UT 2 February substorm.

speed on two sides of the reconnection site (justified by the large variation in magnetosonic speed between the locations of P1 and P5), results in a reconnection onset location of $\sim 23 R_E$ down tail (compared to $\sim 12 R_E$ down tail as obtained by Mende *et al.* [2009]), again consistent with a near-Earth reconnection onset.

[43] Although there is still a long way to go to fully understand the destabilization of the midtail and near-Earth tail, the following points have emerged from our study of the 29 January and 2 February events.

[44] 1. Persistent solar wind V_z or V_y can result in a large tilt of the entire magnetotail. If data are still plotted in the traditional coordinate system under this condition, some key features of substorm signatures may be missed or misinterpreted. One should consider transforming the coordinate system to reveal the true feature of the observation, as we did for the 29 January event.

[45] 2. It is tempting to relate flows directly to substorms and do timing based on the onset time of the flows. For example, the earthward flow onsets at P3 and P4 in the 29 January event are much earlier than dipolarization. However, when the early flows are field aligned, they may be related to plasma sheet thinning before the substorm initiation [Birn and Schindler, 1985] or beams accelerated by the approaching dipolarization front [Zhou *et al.*, 2010]. Cross-field transport and convection do not start until the dipolarization front arrives. Another example is the earthward flow observed at $X_{GSM} = -29.5 R_E$ by P1 during the 29 January event. This fact does not contradict the interpretation that the reconnection site is earthward of P1, because the earthward flow is field aligned and due to an imbalance of counterstreaming beams. This field-aligned flow is consistent with distant-tail reconnection beams.

[46] 3. The azimuthal/vertical propagation of the substorm-related signatures is not a negligible effect. In the 29 January event, both P3 and P4 observed azimuthal flows comparable to earthward flows associated with the substorm. Nonnegligible azimuthal and north-south flows are commonly observed during substorms (R. L. McPherron and T.-S. Hsu, private communication, 2010). The fact that the dipolarization at P3 and P4 is later than at P5 in the 2 February event may be explained by the azimuthal and (more importantly) z direction propagation of the dipolarization front, since P5 was much closer to the neutral sheet than P3 and P4.

[47] 4. We have introduced the hypothesis of different earthward and tailward propagation speeds to the simple method of reconnection site and reconnection time. This assumption is more realistic than the assumption of the same propagation speed on both sides of the reconnection site because the magnetosonic speed earthward of the reconnection site is larger than that tailward of the reconnection site. With the application of this method to the 29 January event and 2 February event, we find that for both events the inferred reconnection site can be around $18\text{--}22 R_E$ down tail with reasonable propagation speeds (200–800 km/s), consistent with earlier studies of substorm triggers [Angelopoulos *et al.*, 2008b; Liu *et al.*, 2009; Gabrielse *et al.*, 2009].

[48] **Acknowledgments.** THEMIS was made possible and is supported in the United States by NASA contract NAS5-02099. Financial sup-

port for the FGM instrument was provided by the German Ministry for Economy and Technology and the German Center for Aviation and Space (DLR) under contract 50 OC 0302. We thank the Canadian Space Agency for logistical support in fielding and data retrieval from the GBO stations. CARISMA is operated by the University of Alberta and is funded by the Canadian Space Agency. GIMA data is provided by the Geophysical Institute of the University of Alaska Fairbanks and the Canadian Magnetic Observatory System (CANMOS) network and maintained and operated by the Geological Survey of Canada, which also provided data used in this study.

[49] Masaki Fujimoto thanks the reviewers for their assistance in evaluating this paper.

References

- Aikio, A. T., V. A. Sergeev, M. A. Shukhtina, L. I. Vagina, V. Angelopoulos, and G. D. Reeves (1999), Characteristics of pseudo-breakups and substorms observed in the ionosphere, at the geosynchronous orbit, and in the mid-tail, *J. Geophys. Res.*, *104*, 12,263–12,288, doi:10.1029/1999JA900118.
- Akasofu, S.-I. (1964), The development of the auroral substorm, *Planet. Space Sci.*, *12*, 273–282, doi:10.1016/0032-0633(64)90151-5.
- Angelopoulos, V. (2008), The THEMIS mission, *Space Sci. Rev.*, *141*, 5–34, doi:10.1007/s11214-008-9336-1.
- Angelopoulos, V., C. F. Kennel, F. V. Coroniti, R. Pellat, M. G. Kivelson, R. J. Walker, C. T. Russell, W. Baumjohann, W. C. Feldman, and J. T. Gosling (1994), Statistical characteristics of bursty bulk flow events, *J. Geophys. Res.*, *99*, 21,257–21,280, doi:10.1029/94JA01263.
- Angelopoulos, V., *et al.* (1995), Growth and evolution of a plasmoid associated with a small, isolated substorm: IMP 8 and GEOTAIL measurements in the magnetotail, *Geophys. Res. Lett.*, *22*, 3011–3014, doi:10.1029/95GL03133.
- Angelopoulos, V., *et al.* (2008a), First results from the THEMIS mission, *Space Sci. Rev.*, *141*, 453–476, doi:10.1007/s11214-008-9378-4.
- Angelopoulos, V., *et al.* (2008b), Tail reconnection triggering substorm onset, *Science*, *321*, 931–935, doi:10.1126/science.1160495.
- Angelopoulos, V., *et al.* (2009), Response to comment on “Tail reconnection triggering substorm onset”, *Science*, *324*, 1391, doi:10.1126/science.1168045.
- Auster, H. U., *et al.* (2008), The THEMIS fluxgate magnetometer, *Space Sci. Rev.*, *141*, 235–264, doi:10.1007/s11214-008-9365-9.
- Axford, W. (1999), Reconnection, substorms and solar flares, *Phys. Chem. Earth, Part C*, *24*, 147–151, doi:10.1016/S1464-1917(98)00022-1.
- Baker, D. N., T. I. Pulkkinen, V. Angelopoulos, W. Baumjohann, and R. L. McPherron (1996), Neutral line model of substorms: Past results and present view, *J. Geophys. Res.*, *101*, 12,975–13,010, doi:10.1029/95JA03753.
- Birn, J., and K. Schindler (1985), Computer modeling of magnetotail convection, *J. Geophys. Res.*, *90*, 3441–3447, doi:10.1029/JA090iA04p03441.
- Birn, J., M. Hesse, G. Haerendel, W. Baumjohann, and K. Shiokawa (1999), Flow braking and the substorm current wedge, *J. Geophys. Res.*, *104*, 19,895–19,903, doi:10.1029/1999JA900173.
- DeCoster, R. J., and L. A. Frank (1979), Observations pertaining to the dynamics of the plasma sheet, *J. Geophys. Res.*, *84*, 5099–5121, doi:10.1029/JA084iA09p05099.
- Eastwood, J. P., D. G. Sibeck, J. A. Slavin, M. L. Goldstein, B. Lavraud, M. Sitnov, S. Imber, A. Balogh, E. A. Lucek, and I. Dandouras (2005), Observations of multiple X -line structure in the Earth’s magnetotail current sheet: A Cluster case study, *Geophys. Res. Lett.*, *32*, L11105, doi:10.1029/2005GL022509.
- Gabrielse, C., *et al.* (2009), Timing and localization of near-Earth tail and ionospheric signatures during a substorm onset, *J. Geophys. Res.*, *114*, A00C13, doi:10.1029/2008JA013583, [printed 115(A1), 2010].
- Ge, Y. S., and C. T. Russell (2006), Polar survey of magnetic field in near tail: Reconnection rare inside $9 R_E$, *Geophys. Res. Lett.*, *33*, L02101, doi:10.1029/2005GL024574.
- Hayakawa, H., A. Nishida, E. W. Hones Jr., and S. J. Bame (1982), Statistical characteristics of plasma flow in the magnetotail, *J. Geophys. Res.*, *87*, 277–283, doi:10.1029/JA087iA01p00277.
- Hones, E. W., Jr. (1980), Plasma flow in the magnetotail and its implications for substorm theories, in *Dynamics of the Magnetosphere, Astrophys. Space Sci. Libr.*, vol. 78, edited by S.-I. Akasofu, pp. 545–562, AGU, Washington, D. C.
- Jacobs, J. A., Y. Kato, S. Matsushita, and V. A. Troitskaya (1964), Classification of geomagnetic micropulsations, *J. Geophys. Res.*, *69*, 180–181, doi:10.1029/JZ069i001p00180.
- Kubyshkina, M., V. Sergeev, N. Tsyganenko, V. Angelopoulos, A. Runov, H. Singer, K. H. Glassmeier, H. U. Auster, and W. Baumjohann (2009), Toward adapted time-dependent magnetospheric models: A simple

- approach based on tuning the standard model, *J. Geophys. Res.*, *114*, A00C21, doi:10.1029/2008JA013547.
- Liu, J., et al. (2009), THEMIS observation of a substorm event on 04:35, 22 February 2008, *Ann. Geophys.*, *27*, 1831–1841, doi:10.5194/angeo-27-1831-2009.
- Liu, J., C. Gabrielse, V. Angelopoulos, N. A. Frissell, L. R. Lyons, J. P. McFadden, J. Bonnell, and K. H. Glassmeier (2011), Superposed epoch analysis of magnetotail flux transport during substorms observed by THEMIS, *J. Geophys. Res.*, doi:10.1029/2010JA015886, in press.
- Lopez, R. E., and A. T. Y. Lui (1990), A multisatellite case study of the expansion of a substorm current wedge in the near-Earth magnetotail, *J. Geophys. Res.*, *95*, 8009–8017, doi:10.1029/JA095iA06p08009.
- Lui, A. T. Y. (1996), Current disruption in the Earth's magnetosphere: Observations and models, *J. Geophys. Res.*, *101*, 13,067–13,088, doi:10.1029/96JA00079.
- Lui, A. T. Y., et al. (2008), Determination of the substorm initiation region from a major conjunction interval of THEMIS satellites, *J. Geophys. Res.*, *113*, A00C04, doi:10.1029/2008JA013424.
- Lyons, L. R., Y. Nishimura, Y. Shi, S. Zou, H.-J. Kim, V. Angelopoulos, C. Heinselman, M. J. Nicolls, and K.-H. Fornacon (2010), Substorm triggering by new plasma intrusion: Incoherent-scatter radar observations, *J. Geophys. Res.*, *115*, A07223, doi:10.1029/2009JA015168.
- Mann, I. R., et al. (2008), The upgraded CARISMA magnetometer array in the THEMIS era, *Space Sci. Rev.*, *141*, 413–451, doi:10.1007/s11214-008-9457-6.
- McFadden, J. P., C. W. Carlson, D. Larson, J. Bonnell, F. Mozer, V. Angelopoulos, K.-H. Glassmeier, and U. Auster (2008), THEMIS ESA first science results and performance issues, *Space Sci. Rev.*, *141*, 477–508, doi:10.1007/s11214-008-9433-1.
- McPherron, R. L. (1979), Magnetospheric substorms, *Rev. Geophys.*, *17*, 657–681, doi:10.1029/RG017i004p00657.
- Mende, S. B., et al. (2008), The THEMIS array of ground-based observatories for the study of auroral substorms, *Space Sci. Rev.*, *141*, 357–387, doi:10.1007/s11214-008-9380-x.
- Mende, S., et al. (2009), Timing and location of substorm onsets from THEMIS satellite and ground based observations, *Ann. Geophys.*, *27*, 2813–2830, doi:10.5194/angeo-27-2813-2009.
- Nagai, T. (2006), Location of magnetic reconnection in the magnetotail, *Space Sci. Rev.*, *122*, 39–54, doi:10.1007/s11214-006-6216-4.
- Nagai, T., M. Fujimoto, Y. Saito, S. Machida, T. Terasawa, R. Nakamura, T. Yamamoto, T. Mukai, A. Nishida, and S. Kokubun (1998), Structure and dynamics of magnetic reconnection for substorm onsets with Geotail observations, *J. Geophys. Res.*, *103*, 4419–4440, doi:10.1029/97JA02190.
- Nagai, T., M. Fujimoto, R. Nakamura, W. Baumjohann, A. Ieda, I. Shinohara, S. Machida, Y. Saito, and T. Mukai (2005), Solar wind control of the radial distance of the magnetic reconnection site in the magnetotail, *J. Geophys. Res.*, *110*, A09208, doi:10.1029/2005JA011207.
- Nishida, A., H. Hayakawa, and E. W. Hones Jr. (1981), Observed signatures of reconnection in the magnetotail, *J. Geophys. Res.*, *86*, 1422–1436, doi:10.1029/JA086iA03p01422.
- Nishimura, Y., L. Lyons, S. Zou, V. Angelopoulos, and S. Mende (2010), Substorm triggering by new plasma intrusion: THEMIS all-sky imager observations, *J. Geophys. Res.*, *115*, A07222, doi:10.1029/2009JA015166.
- Ohtani, S., K. Takahashi, L. J. Zanetti, T. A. Potemra, R. W. McEntire, and T. Iijima (1992), Initial signatures of magnetic field and energetic particle fluxes at tail reconfiguration: Explosive growth phase, *J. Geophys. Res.*, *97*, 19,311–19,324, doi:10.1029/92JA01832.
- Pu, Z. Y., et al. (2010), THEMIS observations of substorms on 26 February 2008 initiated by magnetotail reconnection, *J. Geophys. Res.*, *115*, A02212, doi:10.1029/2009JA014217.
- Richardson, I. G., and S. W. H. Cowley (1985), Plasmod-associated energetic ion bursts in the deep geomagnetic tail: Properties of the boundary layer, *J. Geophys. Res.*, *90*, 12,133, doi:10.1029/JA090iA12p12133.
- Rostoker, G., S.-I. Akasofu, J. Foster, R. A. Greenwald, Y. Kamide, K. Kawasaki, A. T. Y. Lui, R. L. McPherron, and C. T. Russell (1980), Magnetospheric substorms: Definition and signatures, *J. Geophys. Res.*, *85*, 1663–1668, doi:10.1029/JA085iA04p01663.
- Russell, C. T., et al. (2008), THEMIS ground-based magnetometers, *Space Sci. Rev.*, *141*, 389–412, doi:10.1007/s11214-008-9337-0.
- Saito, T. (1969), Geomagnetic pulsations, *Space Sci. Rev.*, *10*, 319–412, doi:10.1007/BF00203620.
- Sergeev, V. A., et al. (1992), A two satellite study of nightside flux transfer events in the plasma sheet, *Planet. Space Sci.*, *40*, 1551–1572, doi:10.1016/0032-0633(92)90052-P.
- Sergeev, V. A., et al. (2000), Multiple-spacecraft observation of a narrow transient plasma jet in the Earth's plasma sheet, *Geophys. Res. Lett.*, *27*, 851–854, doi:10.1029/1999GL010729.
- Shiokawa, K., W. Baumjohann, and G. Haerendel (1997), Braking of high-speed flows in the near-Earth tail, *Geophys. Res. Lett.*, *24*, 1179–1182, doi:10.1029/97GL01062.
- Sibeck, D. G., and V. Angelopoulos (2008), THEMIS science objectives and mission phases, *Space Sci. Rev.*, *141*, 35–59, doi:10.1007/s11214-008-9393-5.
- Slavin, J. A., E. J. Smith, B. T. Tsurutani, D. G. Sibeck, H. J. Singer, D. N. Baker, J. T. Gosling, E. W. Hones, and F. L. Scarf (1984), Substorm associated traveling compression regions in the distant tail: ISEE-3 Geotail observations, *Geophys. Res. Lett.*, *11*, 657–660, doi:10.1029/GL011007p00657.
- Takahashi, K., and E. W. Hones Jr. (1988), ISEE 1 and 2 observations of ion distributions at the plasma sheet-tail lobe boundary, *J. Geophys. Res.*, *93*, 8558–8582, doi:10.1029/JA093iA08p08558.
- Tsyganenko, N. A. (1995), Modeling the Earth's magnetospheric magnetic field confined within a realistic magnetopause, *J. Geophys. Res.*, *100*, 5599–5612, doi:10.1029/94JA03193.
- Wang, C.-P., L. R. Lyons, T. Nagai, and J. C. Samson (2004), Midnight radial profiles of the quiet and growth-phase plasma sheet: The Geotail observations, *J. Geophys. Res.*, *109*, A12201, doi:10.1029/2004JA010590.
- Zesta, E., L. R. Lyons, and E. Donovan (2000), The auroral signature of earthward flow bursts observed in the magnetotail, *Geophys. Res. Lett.*, *27*, 3241–3244, doi:10.1029/2000GL000027.
- Zesta, E., L. Lyons, C.-P. Wang, E. Donovan, H. Frey, and T. Nagai (2006), Auroral poleward boundary intensifications (PBIs): Their two-dimensional structure and associated dynamics in the plasma sheet, *J. Geophys. Res.*, *111*, A05201, doi:10.1029/2004JA010640.
- Zhang, H., et al. (2007), TC-1 observations of flux pileup and dipolarization-associated expansion in the near-Earth magnetotail during substorms, *Geophys. Res. Lett.*, *34*, L03104, doi:10.1029/2006GL028326.
- Zhou, X.-Z., V. Angelopoulos, V. A. Sergeev, and A. Runov (2010), Accelerated ions ahead of earthward propagating dipolarization fronts, *J. Geophys. Res.*, *115*, A00103, doi:10.1029/2010JA015481.

V. Angelopoulos, J. Liu, and C. T. Russell, IGPP/ESS, University of California, Los Angeles, CA 90095-1567, USA. (jliu@igpp.ucla.edu)

K.-H. Glassmeier, Institute for Geophysics and Extraterrestrial Physics, Technische Universität Braunschweig, Braunschweig, D-38106, Germany.

M. Kubyskhina, Institute of Physics, St. Petersburg State University, St. Petersburg, 198504, Russia.

J. McFadden, Space Sciences Laboratory, University of California, Berkeley, CA 94720-7450, USA.